POLITECNICO DI TORINO

Dipartimento di Energetica

Corso di Laurea Magistrale in Ingegneria Energetica e Nucleare

Tesi di Laurea Magistrale

CFD model for tubular SOFC fed directly by biomass

Relatore:

Prof. Massimo Santarelli

Correlatori:

Davide Papurello

Domenico Ferrero

Candidata:

Valentina Somano

ANNO ACCADEMICO 2018 / 2019

ABSTRACT

The increasing energy demand along with the growing attention on environmental issues require a change in the process of energy conversion, that can be accomplished through the exploitation of renewable sources and the development of new, sustainable and efficient technologies.

Among renewable energy sources, biomass presents some positive characteristics: it is cheap, widely spread and can be exploited at any time. Moreover, if used at the same rate as it grows, biomass can be considered as not contributing to CO_2 emission in the atmosphere.

Thanks to the exploitation of the fuel cell technology, it is possible to convert the chemical energy contained in the fuel directly into electrical energy. Not all the fuel cells are able to work when fed with carbonaceous fuels, due to technological issues: solid oxide fuel cells (SOFC) appear to be the best choice, especially in the perspective of an integration between the two features.

In the European context, the DB-SOFC project (Direct Biomass – Solid Oxide Fuel Cell) has been developed in order to exploit the biomass potential for the production of electricity. Integrated in this system, a in situ gasification process of biomass is foreseen to avoid the kinetic restrictions at the anode side, due to the limited contact between the electrolyte and anode electrode and the biomass solid particles.

The aim of this thesis is to create a model for the tubular SOFC: for this purpose, the software COMSOL Multiphysics® 5.3 has been used.

Firstly, the fuel cell operation when fed directly with syngas has been analysed and a comparison between different operating conditions (in terms of pressure and temperature) has been performed, to evaluate the behaviour of the device. After that, the further step has been the implementation of the gasification process and the coupling with the fuel cell, so to describe the complete system.

The simulation of the polarization curves (i-V curves) in the different conditions will represent the goal of the study.

NOMENCLATURE

AU	Air utilization $[-]$
c_p	Heat capacity at constant pressure $[J/(kg \cdot K)]$
d	Characteristic length $[m]$
$D^{eff,f}$	Effective binary diffusion coefficient $[m^2/s]$
D^f	Binary diffusion coefficient $[m^2/s]$
D^K	Knudsen diffusion coefficient $[m^2/s]$
d_{pore}	Pore diameter $[m]$
E	Nernstian voltage $[V]$
F	Faraday's constant $[C/mol]$
FU	Fuel utilization $[-]$
G	Gibbs free energy $[J]$
$\bar{g}$	Molar Gibbs free energy $[J/mol]$
H	Enthalpy $[J]$
$\bar{h}$	Molar enthalpy $[J/mol]$
I	Current $[A]$
i	Current density $[A/cm^2]$
i_l	Limiting current density $[A/cm^2]$
i_{loc}	Local current source $[A/cm^2]$
i_0	Exchange current density $[A/cm^2]$
k	Reaction rate constant $[1/s]$
$\bar{l}$	Molar work $[J/mol]$
M	Molecular weight $[g/mol]$
n_{rds}	Electrons exchanged in the rate determining step $[-]$
p	Pressure $[Pa]$
p_0	Ambient pressure $[Pa]$
Q	Heat $[J]$
R	Rate of reaction $[mol/(m^3 \cdot s)]$
$\bar{R}$	Universal gas constant $[J/(mol \cdot K)]$
Re	Reynolds number $[-]$
S	Entropy $[J/K]$
$\bar{s}$	Molar entropy $[J/(mol \cdot K)]$
T	Temperature $[K]$

u	Velocity $[m/s]$
V	Voltage $[V]$
W	Power $[W]$
z	Charge number $[-]$

GREEK SYMBOLS

α	Charge transfer coefficient $[-]$
β	Simmetry factor $[-]$
ϵ	Porosity $[-]$
ϵ_{ij}	Lennard-Jones characteristic energy $[J]$
γ	Sticking probability $[-]$
Γ	Surface site density $[-]$
η_{act}	Activation overpotential $[V]$
η_{conc}	Concentration overpotential $[V]$
η_{ohm}	Ohmic overpotential $[V]$
μ	Dynamic viscosity $[Pa \cdot s]$
ν	Stoichiometric coefficient $[-]$
ρ	Density $[kg/m^3]$
Σ_{irr}	Entropy due to irreversibilities $[W/K]$
σ	Conductivity $[S/cm]$
$\tilde{\sigma}_{ij}$	Lennard-Jones diameter [Å]
τ	Tortuosity $[-]$
Φ	Heat flux $[W]$
Ω_{ij}	Collision integral $[-]$

ACRONYMS

0D	Zero-dimensional
1D	One-dimensional
2D	Two-dimensional
3D	Three-dimensional
CGE	Cold Gas Efficiency
DGM	Dusty Gas Model
DMR	Dry Methane Reforming
LSM	Lanthanum Strontium Manganite
MCFC	Molten Carbonate Fuel Cell
MIEC	Mixed Ionic Electronic Conductor
OK	Olive Kernel
SMR	Steam Methane Reforming
SOFC	Solid Oxide Fuel Cell
TPB	Three Phase Boundary
WGS	Water Gas Shift
YSZ	Yttria Stabilized Zirconia

LIST OF FIGURES

LIST OF TABLES

INDEX

1. INTRODUCTION

1.1. Description of the project

The increasing energy demand along with the growing attention on environmental issues require a change in the process of energy conversion, that can be accomplished through the exploitation of renewable sources and the development of new, sustainable and efficient technologies. Fossil fuels nowadays cover the great majority of global energy demand and they are expected to continue this trend in the near future. Considering a reference case scenario for the next years up to 2040, projections show the predominance of traditional sources in the production of world's primary energy (that will account for approximately 80% of the total production), although the renewable sources are foreseen to increase with a higher rate. At the same time, from the environmental point of view, world energy-related carbon dioxide emissions will increase with an annual rate of 1.3% from 2010 to 2040 [1]. Such scenario may lead to serious outcomes if a change in the actual global energy system won't be accomplished.

In the energy sector, one of the key themes of last years is the electrification process with proper fuels, that could also result in a considerable green-house gas emissions reduction.

In Europe, in 2016, 239.6 million tonnes of oil equivalent (MTOE) have been consumed in form of electrical energy, nearly 89 MTOE were obtained exploiting renewable energies [2]. The direct production of electricity exploiting renewable energy sources (RES) could represent an interesting path that can be explored.

Among the technologies and the possible energy sources, fuel cells and biomass are becoming more interesting.

In the renewable energy sources landscape, biomass presents some positive characteristics: it is cheap, abundant, widely spread and can be exploited at any time (i.e. it has not an intermittent nature, differently from many others). If used at the same rate as it grows, biomass can be considered as not contributing to CO_2 emission in the atmosphere. Solid biomass, such as agricultural residuals and municipal solid wastes, can be exploited to obtain (thermal) energy through the traditional combustion process, or can be first converted into gaseous or liquid biofuels through, for example, a pyro-gasification process.

Fuel cells, instead, are electrochemical devices that convert the chemical energy contained in the fuel directly into electrical energy. There are different kind of fuel cells, which

differ in terms of operating temperatures. While low temperature fuel cells require pre-processing of fuel as they can work essentially with hydrogen, high temperature ones as solid oxide fuel cells (SOFC) and molten carbonate fuel cells (MCFC) can be fed with carbonaceous fuels. SOFC technology shows the most attractive characteristics [1]. It has a solid-state electrolyte, differently from the molten electrolyte of MCFC, that means no corrosion issues and also the possibility to realize several cell configurations. Moreover, MCFC need carbon dioxide at the cathode side, that represents a further complexity if compared to the SOFC, whose cathode requires air. Finally, the operating temperatures are around 800°C for SOFCs and 600°C for MCFCs: in the perspective of an integration between a fuel cell and the biomass gasification (that is generally carried out at 900°C), for all the characteristics described, the solid oxide fuel cell appears to be the best choice.

If referred to the European context, the Mediterranean countries own more than 85% of world's olive oil production and cultivate large areas with grape vines [3]. This results in a high biomass potential that includes all the residuals from olive and grape vine cultures. Moreover, the exploitation of municipal solid waste is still not developed in these regions, differently from the northern part of Europe. This means the possibility to recover energy from the unused organic fraction of such wastes.

With this in mind, among Euro-Mediterranean countries, the DB-SOFC project (Direct Biomass – Solid Oxide Fuel Cell) has been developed in order to exploit the biomass potential for the production of electricity. Integrated in this system, a in situ gasification process of biomass is foreseen to avoid the kinetic restrictions at the anode side, due to the limited contact between the electrolyte and anode electrode and the biomass solid particles. In this way, it is possible to exploit the high fuel flexibility of SOFC, that is the capability of this kind of cells to work fed with different fuels (not only hydrogen) without the mandatory presence of a pre-reforming stadium.

1.2. Literature review

In the past decades, a number of researchers analysed SOFC systems through mathematical or simulation model, in order to describe the functioning and the performance of the cell. Literature on this technology is quite abundant, with models from zero-dimensional to three-dimensional, with different levels of detail. Although the most analysed case is the SOFC fed with hydrogen, carbonaceous fuel such as carbon monoxide in particular are becoming more interesting and therefore more frequently studied.

The studies on solid oxide fuel cells cover many different features, in order to find more performant materials and operating conditions. The number of studies aiming at describing SOFCs operation through the use of models is increased in the late years. Typically, a SOFC model includes electrochemical, flow and thermal analysis [4]. The physical models of SOFC are usually classified on the basis of the model dimensionality, from 0D to 3D. Generally, 0D and 1D models are applied when the aim of the analysis is the assessment of the optimal operating conditions on system level, with the prediction of steady state and transient performances of the cell and stack, while 2D and 3D models are typically useful for the cell and stack design issues [5]. Typically, low dimension models (0D and 1D) are characterized by less computational time if compared to the high dimension ones (2D and 3D); however, high dimension models are useful to estimate the cell behaviour, in order to find the most appropriate geometry for each particular case study.

Zero-dimensional models are generally used when the single cell is considered as a part of a more complex system. In such cases, the main purpose of the analysis is the estimation of the general performances of the whole system, while physical and chemical parameters variations are not particularly relevant [6].

In one-dimensional model, the fuel cell is usually considered as a set of layers constituting the main components, neglecting the variations at the vertical direction. Aguiar et al. (2004) [7] developed a 1D dynamic model for an anode-supported intermediate temperature planar SOFC. The fuel considered is a mixture of gases including H_2, CO and CH_4, and it is assumed that only hydrogen is subjected to electrochemical oxidation: therefore, the occurrence of water gas shift and methane steam reforming reactions is considered alongside the main electrochemical reaction. This model is able to predict SOFC characteristics both in transient and steady state operations. Concerning the tubular design, Calise et al. (2007) [8] presented a detailed model for the analysis of heat transfer inside a cathode-supported tubular fuel cell. In the study, the fuel cell was discretized along the longitudinal axis. Results showed that radiation heat transfer has a strong influence on temperature distribution.

Two-dimensional models represent an important improvement in the description of the cell behavior, being a simplified form of the 3D models. Xue et al. (2005) [9] presented a dynamic model of a single tubular SOFC unit, for the evaluation of the system behavior and the spatial distribution of state variables under steady state and transient operations. The numerical study is also compared to experimental results, as for the polarization curve, showing quite good agreements.

Three-dimensional models are the most accurate models but also the most time requiring ones. They allow simulating the internal behaviour of the single fuel cell, usually exploiting the finite elements methods to simplify the computation. Results as temperature and fuel distributions can be obtained. Ferguson et al. (1996) [10] developed a 3D mathematical model allowing the computation of the distribution of electrical potential, temperature and chemical species concentration distributions inside the cell. Planar and tubular geometries were compared: according to the analysis, the planar geometry resulted to be the most efficient, showing a lower ohmic losses than the tubular design. Nikooyeh et al. (2007) [11] analysed the operation of a planar SOFC fed with methane, in the presence of internal reforming. The distribution of temperature and gas composition inside the cell were studied. The results highlighted the area of the cell most affected by carbon deposition phenomena and thermal stresses generations. Additionally, the effect of variation in the fuel composition were analysed, observing that a recirculation of anode exhaust gases (up to an optimum value of 60% of recirculation) would lead to a reduction in temperature gradients and in the carbon formation at the anode.

On the other side, gasification is well known and in literature results of various models are available. The models are usually based on thermodynamic equilibrium and kinetics. In general, the thermodynamic equilibrium models assume that all reactions are in thermodynamic equilibrium. They are independent of the gasifier design, but are characterized by a low level of accuracy; the kinetic rate models are more requiring from the computational point of view, but they give more accurate results [12]. An example of kinetic-based model is the one proposed by Gómez-Barea and Ollero (2006) [13], in which the conversions of solid and gaseous materials are reduced to two differential equations, functions of gas and solid reactants concentrations. The process is assumed to be isothermal and quasi steady-state; additionally, the model can be applied to different reactor geometries (slab, cylinder or sphere) and, in principle, can incorporate any kinetics.

As said, thermodynamic equilibrium analyses are independent of the gasifier design, and therefore their application can be more suitable in comparison with the kinetic rate models, that contain precise parameters that can limit their applicability to different case study. However, thermodynamic equilibrium may not be reached, because of the relatively low operating temperatures (from 750 to 1000°C typically) [12]. Nevertheless, such kind of models has been frequently used. Zainal et al. (2001) [14] developed an equilibrium model for downdraft gasifiers, that can be used with different kinds of biomass. They predicted the composition of the producer gas and the relative calorific values for various biomass materials: results highlighted that, with increasing moisture content, the fractions of hydrogen and

methane increase as well, differently from the carbon monoxide, which decreases, and so does the final calorific value.

Although the SOFC and gasification technologies are known and widely studied, the relatively recent argument is the integration between the two features. It can be stated the negative effect of some contaminants on the operation (causing, for example, the deactivation of the nickel catalyst), but a precise analysis is still missing and need further research. Panopulos et al. (2006) [15] developed a model of a SOFC integrated with steam gasification process of biomass, and performed a feasibility study highlighting the main critical aspects, in particular related to the effect of contaminants on the fuel cell operation. The system model was built using Aspen Plus^{TM} simulation software. An electrical efficiency of 36% was obtained, while thermal efficiency was around 14%. Additionally, results showed that high water concentrations inhibit effective H_2S removal at high temperatures, and low temperatures affect negatively the efficiency and cause tar condensation problems. Hayan et al. (2019) [16], instead, developed an exergoeconomic analysis in which the use of air and steam as gasifying agents were compared. The gasification process has been modelled with a thermodynamic equilibrium model. Results showed that, at the optimal operating conditions, when steam is used rather than air, the net output power is increased by almost 15% and the exergy efficiency is increased by almost 25%. However, the effects of contaminants or carbon deposition occurrence have not been considered.

It is therefore clear that, even if the exploitation of producer gas in the fuel cell can be predicted from other analysis, the correct integration and other issues (as the effect of contaminants contained into the syngas on the SOFC operation) are not documented in detail yet [1] and need further analysis.

1.3. Aim of the work

The aim of this thesis is to model the tubular SOFC, analysing firstly the operation when fed directly with syngas. The operation of the syngas-fed SOFC could then be compared to the performances of a theoretical operation considering as fuel pure hydrogen. After that, the further step is the implementation of the gasification process to describe the complete system.

The simulation of the polarization curve (i-V curve) will represent the goal of the study. This will be realized using the software COMSOL Multiphysics® 5.3.

After the design of the cell and the definition of control volume, the operation of the cell will be simulated using the appropriate settings, also considering the parasitic heat generated in

the process. The process will be considered as stationary, in accordance with the real SOFC operation.

Finally, the performances of the system will be analysed, evaluating the efficiency in the operating point, and possible alternatives will be proposed.

2. THEORETICAL BACKGROUND

2.1. Fuel cell: general characteristics

A fuel cell is an open electrochemical cell operating in galvanic regime, i.e. it consumes the chemical energy contained in the reactants (e.g. H_2 and CO) to produce electrical power. The production of electricity is direct, without the intermediate combustion process, and for this reason the efficiency in higher if compared to the traditional methods.

The main components of a fuel cell are the two porous electrodes, which are separated by the electrolyte, as can be seen in Figure 2.1.

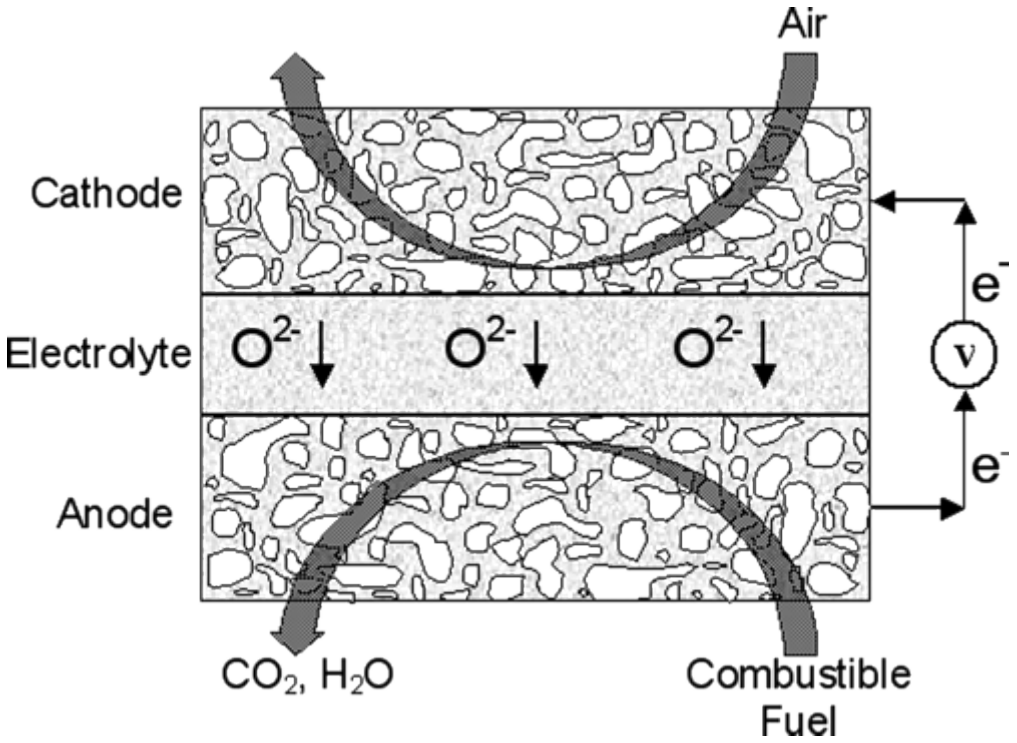

Figure 2.1. SOFC operating principle [17]

The cathode is the positive terminal of the fuel cell, where the reduction reaction occurs: here the oxidant species receives electrons, thus reducing its oxidation number. The anode is, at the contrary, the negative terminal, where the oxidation reaction takes place: the fuel loses electrons, increasing its oxidation number. These two electrodes are physically separated by the intermediate layer called electrolyte. It can be made of solid or liquid material and allows the transfer of ions, preventing the passage of electrons and molecules. It has a key role in the fuel

cell, preventing the direct contact between the anodic and cathodic flows, and characterize the operation of the cell.

In addition to these components, an external circuit connects the two electrodes, in which the electrons are able to flow, creating then a current. In case of series configuration, an interconnector is responsible for electrically connecting cells and letting the current flow, as well as delivering fuels to and removing products from each cell.

So, in this process, a charge separation occurs, leading to the generation of electrical fields on both electrodes: therefore, a voltage differential ΔV is established between the two electrodes. Moreover, the presence of a current I flowing across the voltage gradient will generate electrical power:

$$W_{el} = \Delta V \cdot I \tag{1}$$

The current that is generated in the cell is the Faraday's current and it can be expressed using the Faraday's law:

$$I = \dot{n}_{fuel} \cdot z \cdot F \tag{2}$$

where:

- $\dot{n}_i\ [mol/s]$ is the molar flow rate of species i
- $z\ [-]$ is the number of electrons exchanged in the reaction
- $F = 96486.7\ \left[\frac{C}{mol}\right]$ is the Faraday's constant.

2.1.1. Operation of electrochemical cells

As previously said, fuel cells convert chemical energy of fuels into electricity. This energy contained in reactants should offset the overvoltages rising during the operation, related to reactions activation at electrodes, to ohmic losses and to the decrease of reactants concentration at the site of the reaction. Therefore, if E is the reversible voltage, that is the one related to the amount of energy that the reaction can release in reversible conditions (i.e., in open circuit conditions), the amount of voltage that can produce a useful effect will be:

$$V = E - \eta_{act} - \eta_{ohm} - \eta_{diff} \tag{3}$$

Let's analyse the various contributions to find an analytical formula.

Reversible voltage

The reversible voltage is the voltage that can be measured in open circuit conditions, when there is no current flowing inside the circuit and a chemical equilibrium is established at both electrodes. It is the highest value of voltage that can be obtained from a fuel cell.

To obtain the reversible voltage E it is possible to analyse the fuel cell under the following hypotheses: the fuel cell is represented as a black box, the cell operates in equilibrium conditions (i.e., in reversible conditions) and in steady state. So, it is possible to apply the first and second thermodynamic laws:

$$\begin{cases} \Phi_{th} - W_{el}^{r} = \dot{n}_p \bar{h}_p(T, p_i) - \dot{n}_f \bar{h}_f(T, p_i) - \dot{n}_{ox} \bar{h}_{ox}(T, p_i) = \Delta H_{react} \\ \dfrac{\Phi_{th}}{T} - \Sigma_{irr} = \dot{n}_p \bar{s}_p(T, p_i) - \dot{n}_f \bar{s}_f(T, p_i) - \dot{n}_{ox} \bar{s}_{ox}(T, p_i) = \Delta S_{react} \end{cases} \quad (4)$$

where:

- Φ_{th} $[W]$ is the heat exchanged between the cell with the external environment;
- W_{el}^{r} $[W]$ is the reversible electrical work exchanged by the cell with the external environment;
- $\bar{h}_i(T, p_i)$ $\left[\frac{J}{mol}\right]$ and $\bar{s}_i(T, p_i)$ $\left[\frac{J}{mol \cdot K}\right]$ are, respectively, the molar enthalpy and molar entropy of species *i* at temperature T partial pressure p_i;
- ΔH_{react} $[W]$ and ΔS_{react} $\left[\frac{W}{K}\right]$ are, respectively, the total enthalpy and total entropy of the reaction at temperature and pressure conditions;
- Σ_{irr} $\left[\frac{W}{K}\right]$ is the entropy generated by the irreversibilities and, since we are considering reversible conditions, it is equal zero.

Combining these two equations, it is possible to obtain:

$$W_{el}^{r} = -\Delta H_{react} + T \cdot \Delta S_{react} = -\Delta G_{react} \quad (5)$$

where ΔG_{react} $[W]$ represents the total Gibbs free energy of the reaction. For a galvanic cell, the Gibbs free energy variation is always negative, and therefore the electric power is positive (produced by the cell). Then, normalizing by the molar flow rate of the fuel (6) and exploiting the Faraday's law (7) it can be obtained:

$$\bar{l}_{el}^{r} = -\Delta \bar{h}_{react} + T \cdot \Delta \bar{s}_{react} = -\Delta \bar{g}_{react} \quad (6)$$

$$\bar{l}_{el}^{r} = \frac{W_{el}^{r}}{\dot{n}_{fuel}} = \frac{I \cdot V^{r}}{\frac{I}{F \cdot z}} = V^{r} \cdot F \cdot z \quad (7)$$

The only situation in which the cell is working in reversible conditions is when the circuit is open, in which no transport phenomena occur, and therefore no entropy is generated. The voltage generated in such a situation is called Open Circuit Voltage (OCV), and by combining the two previous equations it can be found the so-called Nernst equation:

$$OCV = -\frac{\Delta\bar{g}_{react}(T, p_i)}{z \cdot F} \quad (8)$$

From this equation, it can be noticed that OCV (the reversible voltage previously called E) depends only on z and $\Delta\bar{g}_{react}$. The dependency on z implies it is affected by the type of reaction occurring, and in particular on the kind of fuel; instead the presence of $\Delta\bar{g}_{react}$ implies a dependence on the thermodynamic state.

The Gibbs free energy is the thermodynamic potential that define the spontaneity of a reaction at defined temperature and pressure conditions, and it reaches a minimum value when the system is in chemical equilibrium. When $\Delta\bar{g}_{react} < 0$, the reaction is spontaneous, as in this case. Being the Gibbs free energy defined as:

$$\Delta\bar{g}_i(T, p_i) = \Delta\bar{h}_i(T, p_i) - T\Delta\bar{s}_i(T, p_i) \quad (9)$$

it is clear that a reaction is spontaneous when it is exothermic ($\Delta\bar{h}_i < 0$) and it is characterized by decreasing order ($\Delta\bar{s}_i > 0$); if it is endothermic ($\Delta\bar{h}_i > 0$) with decreasing order, the reaction will be spontaneous at high temperatures; at the contrary, if it is exothermic but with increasing order ($\Delta\bar{s}_i < 0$), low temperatures will guarantee the spontaneity of reaction. If instead the Gibbs free energy variation is positive, the reaction is not spontaneous, and it will not take place without an external work.

The larger is the Gibbs free energy, the higher will be the voltage drop that can be generated.

If it is then assumed ideal gases model through equation (10), it is possible to explicit the dependence of the OCV on the partial pressure of the various species:

$$\bar{g}_i(T, p_i) = \bar{g}(T, p_0) + \bar{R} \cdot T \ln\left(\frac{p_i}{p_0}\right) \quad (10)$$

$$OCV = -\frac{\Delta\bar{g}_{react}(T, p_0)}{z_f \cdot F} + \frac{\bar{R} \cdot T}{z_f \cdot F} \cdot \ln\left(\frac{\prod_1^n \left(\frac{p_i}{p_0}\right)^{\nu_i}}{\prod_1^m \left(\frac{p_i}{p_0}\right)^{\nu_i}}\right) \quad (11)$$

in which, on the right-hand side, the first contribution can be called standard reversible voltage E^0 and where:

- $\bar{R} = 8.314 \left[\frac{J}{mol \cdot K}\right]$ is the universal gas constant;
- z_f is the number of electrons delivered by the considered fuel;
- m and n are the number of products and reactants, respectively;
- ν_i is the generic stoichiometric coefficient;

- p_0 is the reference pressure.

So, equation (11) represents the expression of the reversible voltage, that can be measured in open circuit conditions, when the current flowing in the circuit is zero. When the circuit is closed, current starts flowing inside the external circuit, breaking the chemical equilibrium that was established at both electrodes. The system it is no more in ideal conditions, and transport phenomena start occurring, with the consequent reduction of the Nernstian voltage for the rising of overvoltages.

Activation overvoltages (η_{act})

The activation overvoltage represents the amount of voltage that has to be spent to overcome the energetic threshold of the activation of the electrochemical reaction. To evaluate this kind of loss the Butler-Volmer equation is used:

$$i = i_0 \cdot \left\{ \exp\left[\frac{\alpha_{an} z F}{RT} \eta_{act}\right] - \exp\left[-\frac{\alpha_{cath} z F}{RT} \eta_{act}\right] \right\} \quad (12)$$

where:

- $i\ \left[\frac{A}{cm^2}\right]$ is the current density produced by the overpotential;
- $i_0\ \left[\frac{A}{cm^2}\right]$ is the exchange current density;
- $\alpha_{an}\ [-]$ and $\alpha_{cath}[-]$ are charge transfer coefficients, for anode and cathode respectively.

Equation (12) must be solved to obtain the value of η_{act} as a function of the current density, to fit it into equation (3). This could be not trivial; therefore, simplification should be assumed. One possibility is to consider $\alpha_{an} = \alpha_{cath}$, in such way the two values of exponential would be equal, and the hyperbolic sinus definition can be exploited. This assumption is reasonable, as the parameters are defined as:

$$\alpha_1 = \beta \cdot n_{rds} \quad (13)$$

$$\alpha_2 = (1 - \beta) \cdot n_{rds} \quad (14)$$

where n_{rds} is the number of electrons delivered in the rate determining step. Actually, a reaction composed by a number of elementary reactions would proceed at the velocity of the slowest one, the rate determining step exactly. β, the symmetry factor, is the fraction of starting potential of the reaction that is used to accomplish the activation: experimentally, it is found being very close to 0.5 in case of electrochemical reactions. Therefore, it is clear that the assumption made on the two parameters α_{an} and α_{cath} is correct. On the basis of these consideration, the expression of the activation overvoltage becomes:

$$\eta_{act} = \frac{R \cdot T}{\alpha \cdot F} \cdot \sinh^{-1}\left(\frac{i}{2i_0}\right) \quad (15)$$

It is important to notice that the Butler-Volmer equation is defined for each half electrochemical reaction, one at the anode and one at the cathode side. Therefore, in the equation (3) there will be present two terms for the activation overvoltages, one for the cathode and one for the anode.

Ohmic overvoltages (η_{ohm})

The ohmic overvoltage is the loss due to both the resistances of electrodes and external circuits to electrons transport and of the electrolytic membrane to ions transport. For this reason, part of the energy has to be used to overcome these resistances and it is lost. This particular loss is described with the Ohm's law:

$$\eta_{ohm} = r \cdot i = \left(r^{el} + r^{ion}\right) \cdot i \quad (16)$$

where r^{el} and r^{ion} are specific resistances in [Ω cm^2]. Between the two terms, the ionic resistance is the prevailing one.

Diffusion overvoltages (η_{diff})

The third term of overvoltage is the diffusion overvoltage, which takes into account the reduction of reactants concentration at the point of the reaction. Actually, the reactants are continuously fed to the cell. However, to reach the electrode/electrolyte interface (the point where the reactions occur), gases have to diffuse inside the porous electrodes: when the current to be delivered increases, higher flow rates are required in order to sustain the higher number of reactions. In such a situation fuel starvage could occur, since the reactants are consumed with a rate higher that the feed one. This leads to a concentration reduction, and therefore to a voltage reduction.

This term can be evaluated using different models: Fick's law, Stefan-Maxwell model and dusty gases model. In this work, the Fick's law is applied, and the overvoltage can be written as:

$$\eta_{diff} = \left|\frac{\bar{R} \cdot T}{z \cdot F} \ln\left(1 - \frac{i}{i_l}\right)\right| \quad (17)$$

in which i_l $\left[\frac{A}{cm^2}\right]$ is the limiting current density, that is the maximum current that can be produced by the electrode. It is written in absolute value, since the logarithmic term is negative, and to maintain an expression similar to the other overvoltage terms. Also in this case, in equation (3) there will be one term for the anodic and one for the cathodic diffusion overvoltages.

Complete expression of voltage

Considering all the contributions evaluated so far, the initial expression of voltage in equation (3) can be rewritten as:

$$V = E_{Nernst} - \eta_{act,an} - \eta_{act,cath} - \eta_{ohm} - \eta_{diff,an} - \eta_{diff,cath} \quad \textbf{(18)}$$

This equation can be represented on a i-V graph with a curve called Polarisation curve. The polarisation curve provides a representation of the performances of a fuel cell: cell voltage is plotted as a function of average current density. The polarisation curve is not unique for a given SOFC: it varies with operating condition (as temperature), reactants adopted and their chemical properties, etc. A typical curve is shown in Figure 2.2. Here the three different regions are well visible, characterized by the three different losses previously described.

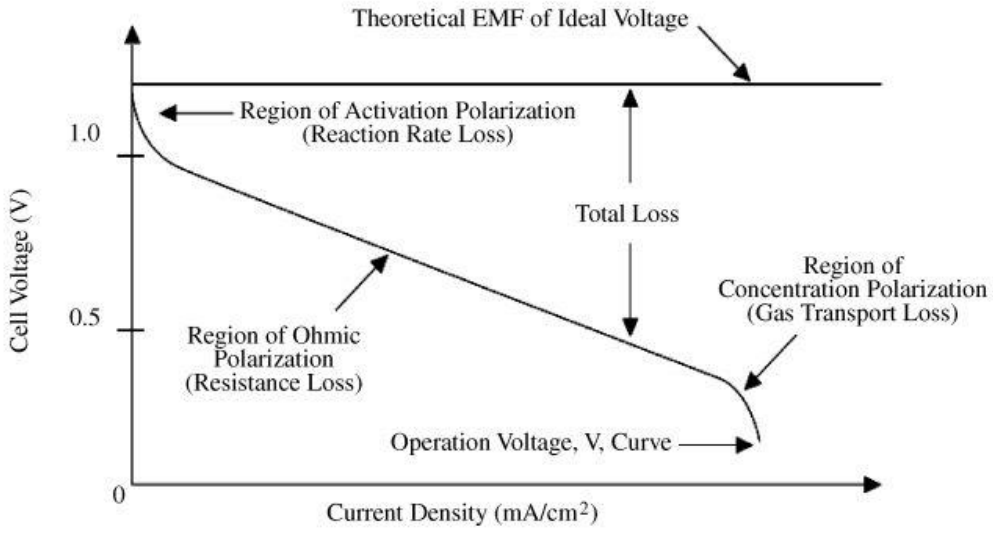

Figure 2.2. Ideal and actual performance of a fuel cell

The fuel cell voltage decreases with increasing values of current density: it starts from the OCV operation point, that is the maximum voltage that can be reached by a fuel cell and is obtained at open circuit conditions. This means that there is no reactant conversion in such a situation.

When the value of current becomes different from zero (closed circuit condition), reactants conversion starts: polarisation phenomena starts occurring, causing voltage drops with respect to the Nernstian value.

2.2. Solid Oxide Fuel Cell

The fundamental device that will be analysed is a Solid Oxide Fuel Cell. It is a high temperature fuel cell, whose typical operating temperatures are around 800°C, and it differs from other fuel cell for the characteristics of its electrolyte, a solid-state component made of mixed oxides of metals and ceramic materials and it is able to transfer O^{2-} ions. A schematic of the operation of the fuel cell is represented in Figure 2.3.

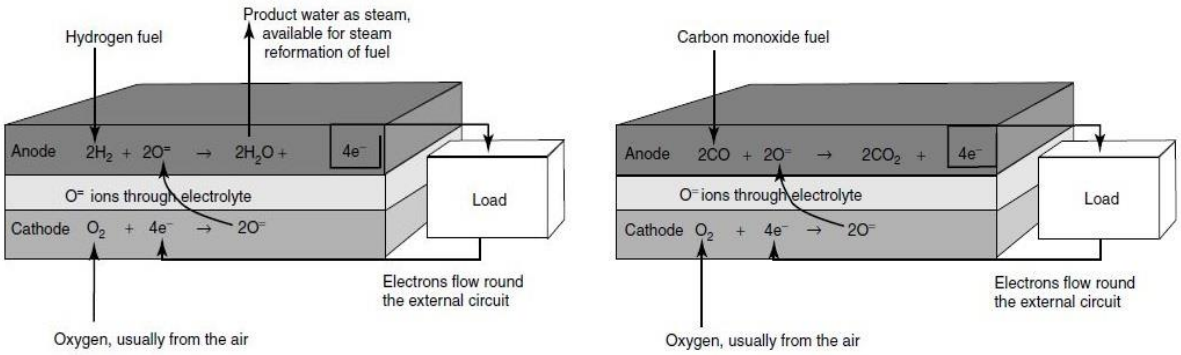

Figure 2.3. Schematic of SOFC operation with H_2 and CO as fuels [18]

2.2.1. SOFC components and materials

The materials considered in this work are the ones at the state of the art.

Electrolyte

The electrolyte is composed by Yttria Stabilized Zirconia (YSZ), that is Zirconium oxide ZrO_2 doped with 8 mole % of Yttrium oxide Y_2O_3. It is nowadays the most effective electrolyte and the most frequently used. It shows a high conductivity of O^{2-} ions in the range between 700°C and 900°C (0.02Scm^{-1} at 800°C), and it can be realized very thin (25-50µm), ensuring low ohmic losses. The high values of operating temperatures guarantee improvement of transport phenomena and the possibility to exploit non-precious catalysts (nickel is the most used nowadays), but at the same time requires the use of high-quality steel for auxiliary components. Other materials considered for the electrolyte layer show higher values of oxygen ion conductivity (as the case of CeO_2), but they are less stable at low oxygen partial pressure. This leads to defect oxide formation and consequently to an increase in the electronic conductivity: this would cause the increase of the internal current, which decreases the potential of the cell (cross-over effect). Such issue does not occur in case of YSZ electrolyte.

Anode

The anode is constructed from Cermet, an alloy of metallic nickel and a ceramic (YSZ, the same of the electrolyte) skeleton. Nickel works both as catalyst and electronic phase. The anode has a high porosity (generally 20-40%), that make easier the mass transport of reactant and product gases. The ohmic polarisation losses that arouse at the interface between anode and electrolyte push for a further investigation on bi-layer anodes in order to reduce such losses.

Cathode

The cathode is instead constructed from a Mixed Ionic Electronic Conductor (MIEC) material, called Perovskite: in particular a strontium-doped lanthanum manganite (LSM) it is considered, with the general formula $La_{1-x}Sr_xMnO_3$. LSM is a p-type semiconductor, with good ionic and electronic conductivity. Also this component is characterized by a porous structure, for the same reasons already seen for the anode.

Other components

Alongside these three main components, other parts are needed for a correct operation of the cell and the stack. The interconnect is the components that electronically connect neighbouring cells, and that in tubular SOFCs has a particular design. It can be made of different materials; ceramic ones are preferred for the tubular design. It should be dense, to avoid molecular diffusion, a good electronic conductor and it must guarantee good mechanical and structural properties even at high temperatures. Nowadays the most promising material is Crofer 22 APU, a ferritic stainless steel doped with 22 wt% chromium.

Then fundamental importance is given to the sealing material, to obtain gas-tightness and thus preventing gas leakages. Material choice is not trivial: it must guarantee good adhesion both with ceramic material and metal. Usually it is constructed from glass-ceramic materials, which suffer from thermal cycles.

2.2.2. Practical design

For which concern the geometry, the absence of a liquid phase layer simplifies the cell configuration and allows the development of different cell geometries. There are typically two different SOFC typologies: planar and tubular fuel cells. A schematic configuration is shown in Figure 2.4. Moreover, the mechanical stiffness is granted increasing the thickness of one of the three layers: there will be so anode supported, cathode or electrolyte supported cells. The construction process varies according to the kind of cell selected.

In order to give sufficient strength to the cell, supporting component should be thick enough. In general, for high temperature SOFC electrolyte support is desirable, since ionic

conductivity of electrolyte increases with temperature: the increase in ohmic drop due to the thicker electrolyte layer would be then counteracted.

In typical operating conditions, a single cell can produce a voltage lower than 1V. Higher values of voltage and therefore of power extracted are reached by connecting cells together in a stack, using series and parallel connections.

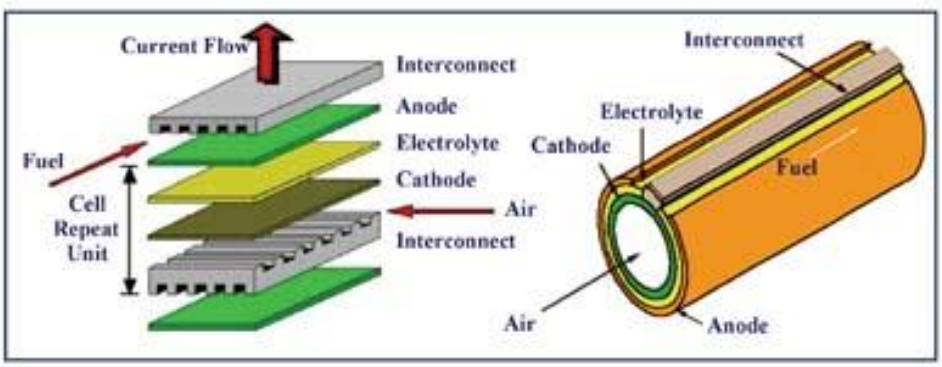

Figure 2.4. Schematic configuration of a planar and a tubular cell [19]

Tubular design

The tubular designed was first realized by US Westinghouse Electric Corporation (now Siemens Westinghouse) in the late 1970s. Even if the main issue with tubular SOFCs is the expensive fabrication process, a great advantage of such configuration is the elimination of high temperature gas leakages: actually each tube (as in the modelled configuration) is closed at one end: fuel flows along the external side of the tube, while oxidant (air) is injected in the internal side through a thin alumina tube located in the central part of each cell. To obtain a useful amount of electrical power, cells are connected in parallel and series connection, to create a bundle, that is the base unit of the generator: the bundles then are connected between them in series. The connections are realized using a wire made of nickel.

In this work the analysed SOFC is a tubular, electrolyte supported cell.

Planar design

An alternative configuration is the planar design, in which the components are flat plates connected in series. Nowadays, development in the materials research makes planar SOFC more interesting. The main problematics related to this configuration are related to the gas flows inside the cell and the gas leakages; on the other side, the construction process is simpler and less expensive. Also, planar configuration guarantees a more compact design and simpler electrical connection between cells.

2.2.3. Morphology of the cell

The morphology is particularly important for the correct operation of the cell. Electrodes must be sufficiently porous to allow a good diffusion of gases inside the layer, up to the electrolyte interface. At the same time, products must be rapidly removed, to minimize diffusivity problem: in the case of SOFC, particular importance must be given to the anode side, where there is the formation of reaction products. Moreover, the stiffness must be high enough to withstand the mechanical stresses and avoid the break of the cell. Then, the use of syngas (mixture of hydrogen and carbon monoxide) requires high level of reactivity of the material, that for this reason must present a sufficient active surface area per unit volume.

More precisely, the morphology of the electrolyte/electrode interface is a fundamental aspect, since it is the region where the electrochemical reactions occur. This region is characterized by the coexistence of three different phases: the porous phase, through which the molecules of reactants are supplied, and the products are removed, the electrolytic phase, that removes and supplies by the O^{2-} ions, and the metallic phase, that removes and supplies electrons. The point in which these three phases coexist is called Three Phase Boundary (TPB). A representation of such a region is shown in Figure 2.5.

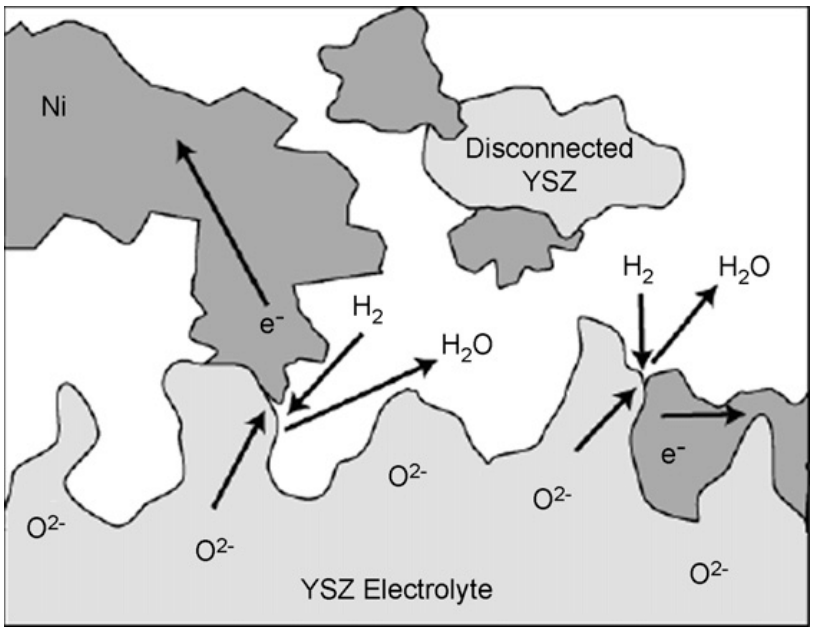

Figure 2.5. Schematic representation of Ni-YSZ TPB region (anode side) [31]

As a consequence, fine-grain electrode will perform better, guaranteeing a higher TPB surface.

2.2.4. Effect of high temperature on SOFC operation

As previously said, SOFCs are high temperature fuel cells characterised by operating temperatures in the range of 750-1000°C. High temperatures reached have positive and negative effects.

The main advantage is the improvement in the transport phenomena, that decreases the polarisation overvoltages. Electrode kinetic is improved, with consequent faster reactions, therefore the activation overvoltages are reduced. Moreover, electrolyte ionic conductivity as said increases with higher temperature, and so also ohmic overpotential are counteracted.

Additionally, higher operating temperature means higher quality exhaust heat, that can be further exploited.

On the other hand, high temperatures lead to some problematics. Related to the materials of auxiliary components, highly resistant steels have to be used to withstand corrosion phenomena and maintain mechanical and thermochemical properties integer. For which concern the operating phase, high temperature implies slower start-up and shut-down: SOFC are not designed to work in transitional regimes, but rather for continuous stationary operations.

2.2.5. SOFC operation with hydrocarbons

One of the most important characteristics that make SOFCs so interesting among the other fuel cells is their fuel flexibility, that is their capability to work fed with a variety of fuels. This is due mainly to the high temperatures (700-1000°C) reached in the operation and the consequent possibility to use non-precious catalyst, like Nickel, that do not suffer from poisoning effects related to carbon presence. For these reasons, a syngas-fed SOFC can be an interesting application.

The possibility to exploit a great variety of fuels presents some positive and negative effects. The possibility to use fuels with higher reversible potential and the higher ideal efficiencies, the simplification of the plant (that won't necessarily need any more external reformers for example) are the main advantages. On the other hand, anode deactivation due to carbon deposition and, in general, the presence of impurities could lead to degradation of the electrode and therefore problems during the operating life of the device.

Let's analyse these aspects.

In this work, three fuels have been considered: hydrogen, carbon monoxide and methane, contained in different fractions into the syngas produced after the biomass gasification. The reaction with the highest rate of kinetics at the Ni-YSZ anode is the hydrogen,

while the carbon monoxide has a slower activation. Methane can react directly at the anode also, but proper catalysts are needed, as cerium.

The electrochemical reactions that can occur at the anode electrode, where there is the oxidation reaction, are the following:

$$H_2 + O^{2-} \rightarrow H_2O + 2e^- \quad (19)$$

$$CO + O^{2-} \rightarrow CO_2 + 2e^- \quad (20)$$

$$CH_4 + 4O^{2-} \rightarrow 2H_2O + CO_2 + 8e^- \quad (21)$$

At the cathode the only reduction reaction is the oxygen reduction:

$$O_2 + 4e^- \rightarrow 2O^{2-} \quad (22)$$

Different fuels mean necessarily different thermodynamic properties and therefore different Nernstian potentials. From literature, equations of state able to express enthalpy and entropy as function of temperature and pressure are available for ideal gases. From these equations it is possible to calculate the standard reversible potential and obtain:

TOTAL REACTION	REVERSIBLE VOLTAGE E^0 [V]	
$\boldsymbol{H_2 + 0.5\, O_2 \rightarrow H_2O}$	$E^0 = \frac{\Delta g}{2F}$	0.978
$\boldsymbol{CO + 0.5\, O_2 \rightarrow CO_2}$	$E^0 = \frac{\Delta g}{2F}$	0.980
$\boldsymbol{CH_4 + 4\, O_2 \rightarrow 2\, H_2O + CO_2}$	$E^0 = \frac{\Delta g}{8F}$	1.038

Table 2.1 Reversible voltages at 800°C and 1 atm of the considered reactants

Table 2.1 shows a higher reversible voltage (at 800°C and 1 atm) using methane. This leads to an important advantage: a fuel with higher value of Gibbs free energy variation allows to reach a higher value of ideal efficiency, since it is defined as:

$$\eta_{id} = \frac{\Delta G_{react}}{\Delta H_{react}} \quad (23)$$

Such efficiency is not reachable during normal operation, since the reversible voltage is obtained in case of open circuit operation but represents a theoretical limit.

However, the use of carbonaceous fuel can lead to some problematics. The simultaneous presence of high operating temperatures and nickel catalyst promotes the degradation of carbonaceous molecules, such as CO and CH_4, into solid carbon, on the basis of three reactions, the methane cracking (24), the reverse Boudouard reaction (25), and the reduction of carbon monoxide (26):

$$CH_4 \rightarrow C + 2H_2 \quad (24)$$

$$2CO \rightarrow C + CO_2 \quad (25)$$

$$CO + H_2 \rightarrow C + H_2O \quad (26)$$

As a consequence of these three reactions, carbon deposition will occur over the anode surface, deteriorating the catalytic activity of Ni-Cermet electrode and obstructing the pores of the anode, thus preventing the fuel molecules from reaching the TPB region and reacting with O^{2-} ions. In addition to this, in absence of fuel, oxygen will oxidize nickel atoms, generating NiO: it occupies a bigger volume than Ni, therefore it will increase the mechanical stresses inside the dense electrolyte layer, which can be walking into a rupture. In order to avoid such problems, the diffuse solution is to add water vapour to the fuel, to maintain its partial pressure sufficiently high to activate the reaction:

$$C + 2H_2O \rightarrow CO + 2H_2 \quad (27)$$

that is able to counteract the previous three. Moreover, fuel processing reactions can occur too: they are reaction of fuel conversion, in this case hydrocarbons conversion, that in presence of water vapor and with high temperatures can react and produce H_2. Two main reactions can be considered. The first one is the steam methane reforming (SMR), the catalytic conversion of methane in a H_2-rich gas, according to the reaction:

$$CH_4 + H_2O \rightarrow 3H_2 + CO \quad (28)$$

Reforming processes can occur both at the anode side and in a separated device integrated in the SOFC stack: in both cases we can talk about internal reforming. The internal reforming allows the complete system efficiency to increase and reduces the overall complexity of the plant, since a lower number of devices is needed. Since the molar fraction of methane in the syngas composition considered is particularly low (with percentages equal to or lower than 0.1%) and the nickel is a catalyst for the reforming reaction, the methane has been assumed not electrochemically reacting with O^{2-}ions but only taking part in the SMR reaction to produce the other two fuels.

Carbon monoxide produced in the SMR can electrochemically react at the anode, however the favoured reaction is the water gas shift (WGS) reaction, in which the carbon monoxide reacts with water vapor leading to the formation of further hydrogen:

$$CO + H_2O \rightarrow H_2 + CO_2 \quad (29)$$

The water vapor necessary for these two reactions can be obtained by the products of electrochemical reactions (that is the hydrogen oxidation), alongside the amount of water recirculated exploiting the anode exhaust.

Moreover, the biomass gasification could cause the formation of tars, that would create problem in the SOFC operation.

2.3. Biomass conversion

The other main feature of the project is the biomass gasification, that would be accomplished directly at the anode side to produce syngas.

In general, gasification is a thermochemical process in which a carbonaceous fuel is partially oxidized in a condition of lack of oxidant agent. The aim of such process is to improve the fuel quality and therefore increase the efficiency of its thermochemical conversion. Moreover, as said before, in this particular application gasification is needed to prevent the limited contact between the electrolyte and anode electrode and the biomass solid particles, that would decrease the kinetic of the reaction.

The product of the gasification process is the syngas, a gas mixture composed mostly by CO and H_2 in varying ratios. Gasification needs the presence of an external agent to perform the partial oxidation of the carbonaceous compounds. The main oxidant agent used are oxygen (or air), water vapour and carbon dioxide. The process requires heat which is supplied by the partial oxidation reactions.

In order to understand the advantages and issues related to this process it is useful to analyse the primary source that will be exploited, the biomass.

2.3.1. Biomass

The term biomass can be referred to any kind of organic material with direct vegetal or animal origin (primary biomass), but also the biodegradable fraction of municipal solid waste, waste water, and agricultural waste, etc. Among primary biomass, lignocellulosic one is the most spread, and its main constituents are cellulose, hemicellulose, lignin; then, minor amounts

of extractives and ashes are present. Lignocellulosic biomass has a complex structure in which cellulose fibres are surrounded by a layer of hemicellulose and embedded in a matrix of hemicellulose and lignin.

Of course, biomass composition can also be expressed in term of elementary constituents, i.e. carbon, dry matter and moisture. A typical composition is shown in Figure 2.6. As can be seen, the percentage of the elementary components varies deeply according to the particular biomass feedstock taken into account.

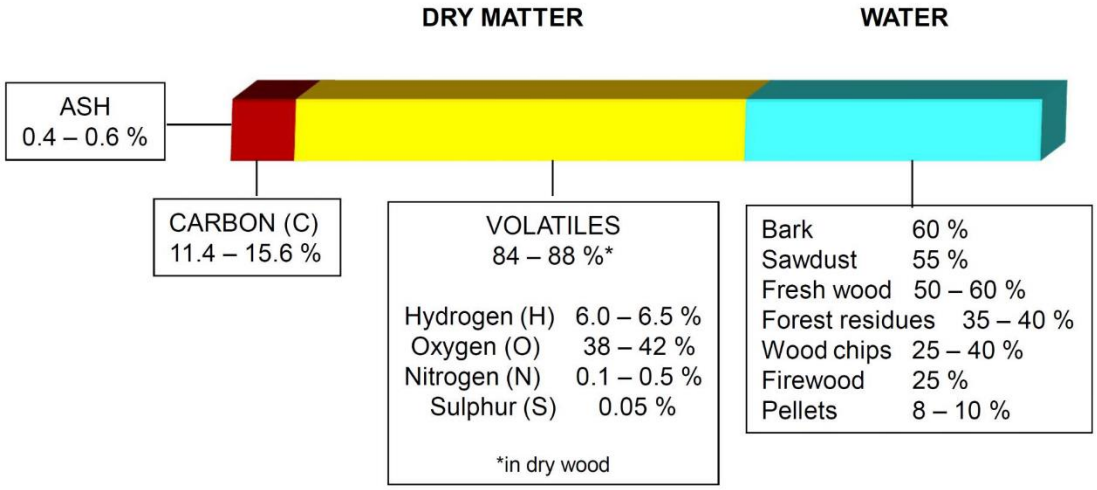

Figure 2.6. Typical biomass composition

As outlined before, the biomass exploited in this project is a mixture of olive kernel, pruning from olive oil and grape vines and the biological fraction of municipal solid waste. In the model, olive kernel is considered as the main component of initial feedstock.

From an energetic point of view in particular, nowadays biomass is becoming more interesting. The production of the so-called biofuels (in liquid or gaseous form) is knowing an important increase in the last decade, as it can be seen in Figure 2.7. Global biofuels production increased by 3.5% in 2017; the largest increment is due to the US, but globally the overall production is more than doubled. The main reasons that make this source interesting are its predictability, not always ensured with RES, and that it is a renewable carbon source. On the other hand, its great volumes and the low ratio LHV/weight make it not so easily exploitable in an efficient way. Therefore, a further process can be useful to obtain higher quality fuels.

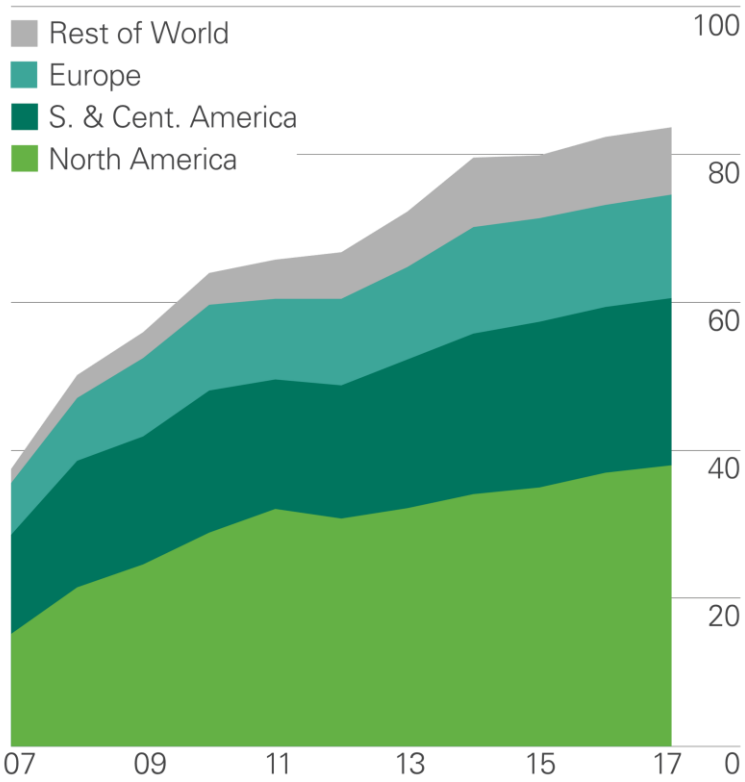

Figure 2.7. World biofuels production by region from 2007 to 2017 (million tonnes of oil equivalent) [20]

Biofuels can be obtain processing the starting biomass following two different paths: through biochemical conversion or thermochemical conversion. Both methods aim at the production of liquid or gaseous biofuels with higher energy content; the biochemical conversion requires more time than the thermochemical one, that is much faster.

In this work, biomass conversion into gases will be accomplished through the thermochemical process of gasification.

2.3.2. Gasification process

In general, the gasification process requires a series of step, occurring at different temperatures:

- Pre-heating and drying (<200°C);
- Pyrolysis (200-600°C);
- Gasification (600-1000°C);
- Combustion (1000-1500°C).

Although considered in a separated way, in real processes there can be a superposition in the occurrence of these steps. Let's analyse each one.

Pre-heating and drying

As previously observed, the moisture content of biomass is quite variable, from about 8-10% to very higher values of about 50-60%. From an energy view point, this can result in a sharp drop of conversion efficiency: for each kg of moisture contained in the starting biomass an amount of roughly 2300 kJ is needed to vaporize such water. This energy will be lost and cannot be used to sustain the gasification process. That is why this first step is so important to obtain syngas with high quality heating value.

Pyrolysis

Pyrolysis is a thermochemical degradation of biomass carried out in total absence of oxygen or any other oxidizing agent, in which large hydrocarbon molecules break down into relatively smaller and simple molecules. The products of such process are charcoal (solid), bio-oil (liquid) and gas. Depending on operating the condition, different pyrolysis processes are possible, which result in different final products. In any case, temperatures higher than 400°C are generally required.

Gasification and combustion

The real gasification takes place in the reduction zone, where the pyrolysis products react with the oxidizing agent. Those reactions are carried out in lack of oxygen, to prevent the occurrence of combustion reactions, that will lead to the production of exhaust gases, useless for a further exploitation.

The main reactions taking place are summarized in Table 2.2.

All reactions lead to the production of the syngas, excepts for the oxidation reactions (R5-8). All reactions with oxygen are essentially complete, under the assumption of gasification conditions (low amount of oxygen mean it will surely react totally). Reaction R1, R2 and R13 are the only endothermic ones, while the others are exothermic. Oxidation reactions (that are combustion reactions) have a fundamental role in the overall process, since they provide the heat required to sustain all the other steps (heating, drying and pyrolysis).

TYPE OF REACTION	STOICHIOMETRIC REACTION	
Carbon reactions	**Reaction**	**ΔH_{react} (T=25°C)**
R1	$C + CO_2 \leftrightarrow 2\,CO$	+172 kJ/mol
R2	$C + H_2O \leftrightarrow CO + H_2$	+131 kJ/mol
R3	$C + 2\,H_2 \leftrightarrow CH_4$	-74.8 kJ/mol
R4	$C + 0.5\,O_2 \rightarrow CO$	-111 kJ/mol
Oxidation reactions		
R5	$C + O_2 \rightarrow CO_2$	-394 kJ/mol
R6	$CO + 0.5\,O_2 \leftrightarrow CO_2$	-284 kJ/mol
R7	$CH_4 + 2\,O_2 \rightarrow CO_2 + 2\,H_2O$	-803 kJ/mol
R8	$H_2 + 0.5\,O_2 \rightarrow H_2O$	-242 kJ/mol
Water gas shift reaction		
R9	$CO + H_2O \leftrightarrow CO_2 + H_2$	-41.2 kJ/mol
Methanation reactions		
R10	$2\,CO + 2\,H_2 \rightarrow CH_4 + CO_2$	-247 kJ/mol
R11	$CO + 3\,H_2 \leftrightarrow CH_4 + H_2O$	-206 kJ/mol
R12	$CO_2 + 4\,H_2 \rightarrow CH_4 + 2\,H_2O$	-165 kJ/mol
Steam reforming reactions		
R13	$CH_4 + H_2O \leftrightarrow CO + 3\,H_2$	+206 kJ/mol
R14	$CH_4 + 0.5\,O_2 \rightarrow CO + 2\,H_2$	-36 kJ/mol

Table 2.2. Gasification reactions

2.3.3. Effects of biomass composition on gasification process

The particular composition of biomass affects significantly the gasification step.

Firstly, as already seen, high moisture content (roughly, higher than 40 wt%) decreases the process conversion efficiency, and also the final composition and heating value of syngas. However, some water content is desirable since the steam produced thanks to the high temperatures will act both as gasifying agent in the syngas production and as reactant in the water gas shift reaction, increasing the H_2/CO ratio in the producer gas. A drying process in an external device, prior to the gasification chamber, can be useful; therefore, it is costly. In the perspective of an integration with a SOFC, a recirculation of the hot exhaust of the fuel cell can be introduced to guarantee a higher level of dehydration without an excessive increase the costs.

However moisture is not the only source of issues: also ashes have to be taken into account.

The higher the ash content, the more important can be the issues, as the occurrence of corrosion phenomena of the external walls and the prevention of chemical reactions.

2.3.4. Effects of biomass composition on SOFC operation

Besides the impurities depositions that can clog the anode surface of SOFC, biomass composition can affect SOFC operating in particular through the consequent syngas composition. Producer gas can contain particulates, ashes, tar, and also alkali, sulphur, chlorine and nitrogen compounds.

Considering this system, the occurrence of the gasification directly at the anode side makes impossible the insertion of a cleaning step before the fuel injection in the cell. The SOFC response to the presence of syngas impurities differs according to the material chosen for the anode (the electrode in which the fuel is injected).

Particulates are to be reduced as much as possible. Their size could be in the order of μm or lower; anode pores dimensions are in the same order, therefore they could be blocked by them, preventing the fuel diffusion inside the porous structure and reducing the anode catalytic area. This could cause irreversible degradation of the cell.

Instead, while they can be considered as not poisonous for SOFC, tars can lead to deactivation of the nickel catalyst due to carbon deposition and cell degradation. From the current literature, it is possible to assume that the tolerance level of tar in the syngas in a SOFC with a Ni-YSZ anode is roughly a few ppm.

Concerning the sulphur compounds, it is widely studied their effect on SOFC operation. Sulphurs are converted into H_2S, which deactivate the active sites. Even a low amount of H_2S (few ppm) is poisonous for the cell therefore highly affecting its performances, increasing the polarisation resistance; high levels instead will cause irreversible damages.

For other impurities scarce literature is found, demonstrating in general their responsibility in the reduction of performances of the cell.

2.3.5. Gasification results

In previous work packages of the DB-SOFC a catalytic evaluation for the bio-gasification has been performed. In this work the results of such previous analysis will be used to initially define a possible composition for the syngas entering the fuel cell.

The reactivity of selected biomass (olive kernel, OK) and its biochars has been determined at University of Western Macedonia in collaboration with Technical University of Crete, under different operating temperature. It has been analysed under both inert (He) and

reactive (H_2O, CO_2) atmospheres. The best results have been obtained with H_2O and CO_2; therefore, these results will be taken into account. Such results are shown in Figure 2.8 below. The graphs show the effect of temperature on the outlet composition during the gasification of biomass at 300°C (identified with OK300), 500°C (OK500), and 800°C (OK800). Since the operating temperature in stationary state will be 800°C, the related composition is considered.

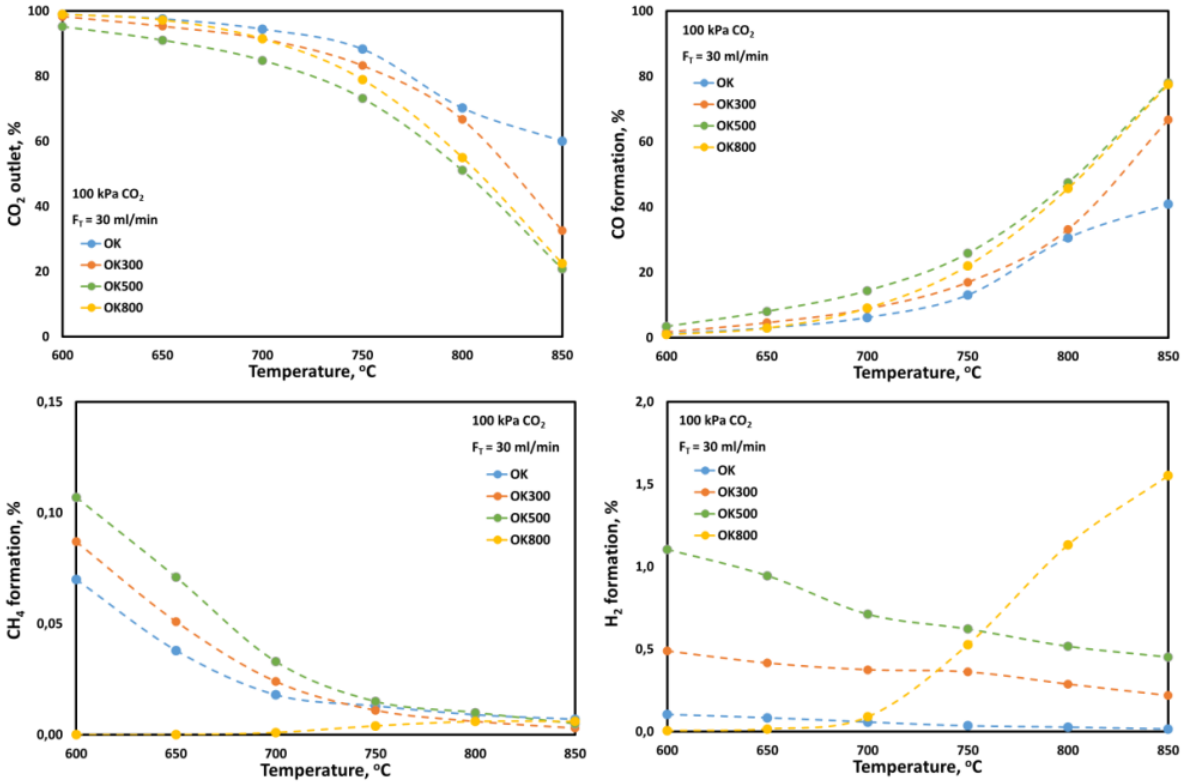

Figure 2.8. Effect of temperature on CO_2, CO, CH_4 and H_2 outlet concentrations in different operating conditions using CO_2 as gasifying agent

So from the graphs, the concentrations of CO_2, CO, H_2 and CH_4 can be obtained on a dry basis. In Table 2.3 the considered concentrations at gasification temperature of 800°C can be observed.

COMPOUND	OUTLET CONCENTRATION AT 800°C [v%]			
	OK	**OK300**	**OK500**	**OK800**
CO_2	69.94	66.64	52.44	55.7
CO	30	33	47	43
CH_4	0.05	0.1	0.05	0.1
H_2	0.01	0.26	0.51	1.2

Table 2.3. Outlet syngas concentrations on a dry basis at different olive kernel temperatures

The amount of moisture in syngas is considered to be the same of the biomass. The percentage has been obtained from literature and has been assumed as 10 wt%.

Assuming a working temperature of the SOFC of 800°C, it is coherent the analysis of the syngas composition considering the concentrations obtained through the gasification of the olive kernel at the same temperature.

3. THE MODEL

In order to correctly model the SOFC operation and the gasification process, several equations have been applied. For the description of the electro-kinetic phenomena occurring at the electrode/electrolyte interface layer, equations proposed in literature have been introduced. For a correct simulation, an analysis on literature data has been carried on: therefore, the correlations chosen are referred to similar components (SOFCs, when possible tubular cells), materials (Ni-YSZ, LSM and YSZ for anode, cathode and electrolyte) and operating conditions.

In this chapter the main representative equations are shown; for a better understanding, some of the equations already seen in the previous chapter will be re-written. Additionally, the geometrical and morphological parameters of the fuel cells alongside to other descriptive parameters are presented.

3.1. SOFC model and design

The simulation realised is based on some simplifying hypotheses, for which concerns both the design and the working mechanisms of the fuel cell.

The model simulates the operation of a single tubular SOFC, close at one end, with the cathode electrode at the internal side and the anode at the external one, separated by the solid electrolyte. The air is injected in the internal side to reach the cathode electrode, while the fuel is supplied through the external layer. The fuel cell geometry has been realized exploiting the axisymmetric nature of the cell, using therefore a 2D-axisymmetric component. The design is shown in Figure 3.1, while in Figure 3.2, an enlargement of the thinner layers can be seen. As it can be noticed, the thin cell structure is inserted inside a bigger region, that can be thought as a control volume, in order to represent the cathodic and anodic flow channels, where the reactants are supplied, and the products can be removed.

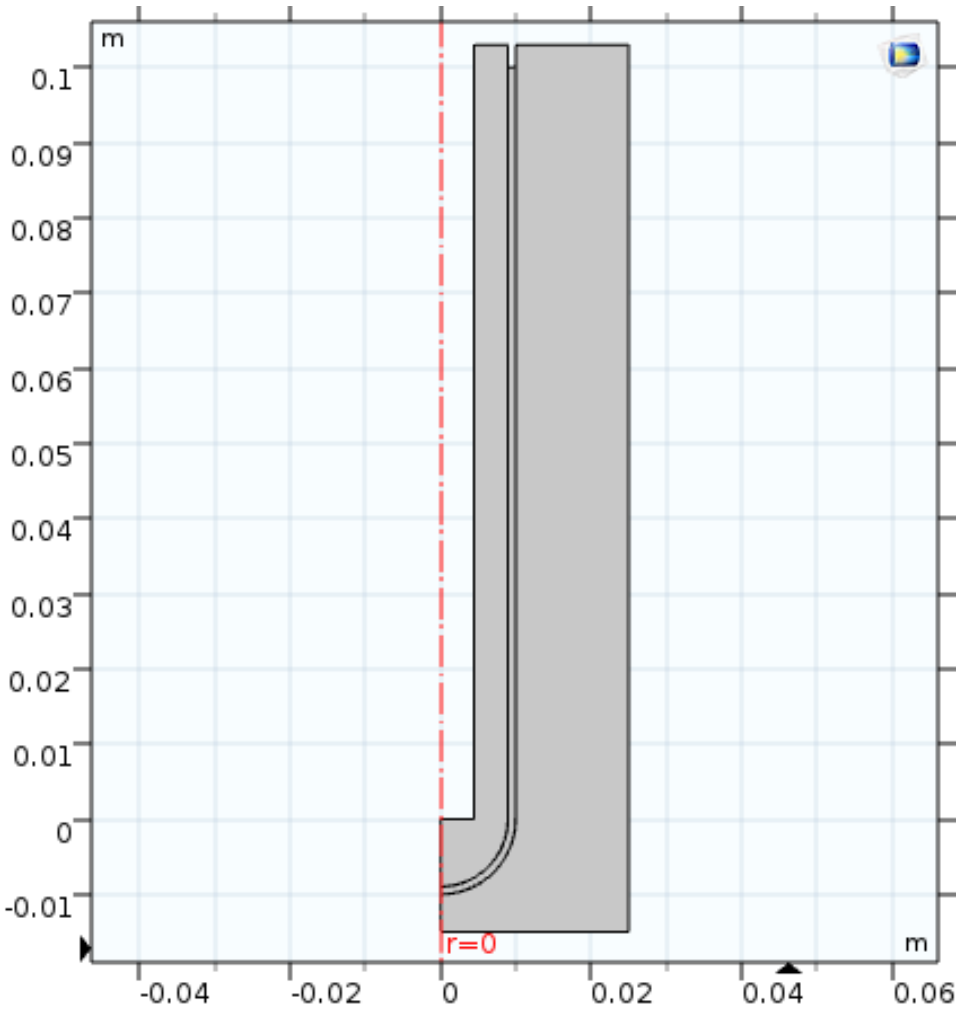

Figure 3.1. SOFC geometry on COMSOL Multiphysics® 5.3

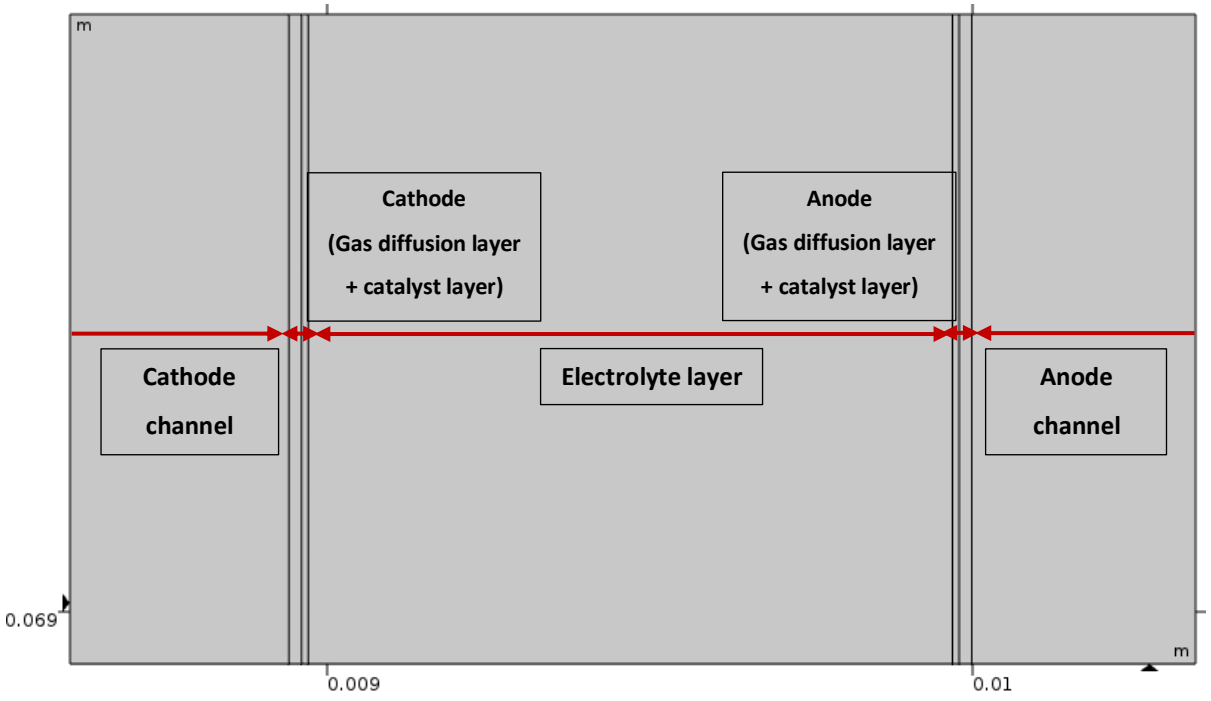

Figure 3.2. Zoom on the layers of the fuel cell

In the COMSOL model of the SOFC, as it can be seen in Figure 3.2, the three main components have been represented: the two electrodes, constituted by a gas diffusion layer and a thinner active layer, and in between the electrolyte layer. Since the software needs different boundaries for flows inlet and outlet, the internal side of the cell presented the issue related to the fact that the air is supplied and removed from the same section. To avoid this problem, the internal side of the cell has been thought as composed by a thin tube (whose diameter is about half of the fuel cell diameter) from which the air can be injected: this possible design finds validation from some documents in literature, therefore it is used in this work. Additionally, the internal feeding tube could constitute also an air pre-heating component. The 3D geometric design of the cell with the gas flows would be as shown in Figure 3.3.

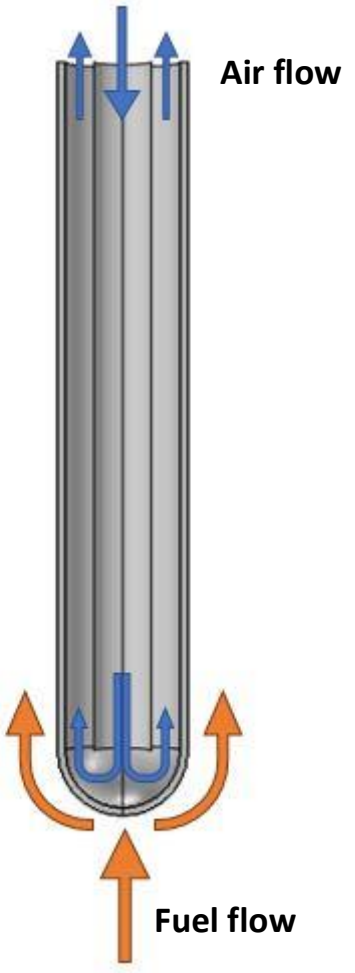

Figure 3.3. Gas fluxes represented in the 3D geometry

The geometrical and morphological parameters are listed in Table 3.1: the latter (such as porosity and tortuosity) have been found from literature [21]. In table, instead, the values of conductivity for electrolyte and electrodes material are shown.

TUBE	
Diameter	2 cm
Length	10 cm
Thickness	ca. 1 mm
ANODE ***Material: Ni-YSZ***	
Thickness	30 μm
Catalyst layer thickness	10 μm
Specific catalyst area	1080 cm^{-1}
Porosity, ϵ	0.3
Tortuosity, τ	3
CATHODE ***Material: LSM***	
Thickness	30 μm
Catalyst layer thickness	10 μm
Specific catalyst area	1080 cm^{-1}
Porosity, ϵ	0.335
Tortuosity, τ	5
ELECTROLYTE ***Material: YSZ***	
Thickness	1 mm

Table 3.1. Geometrical and morphological cell parameters

MATERIAL	SPECIFIC IONIC CONDUCTIVITY, σ	SPECIFIC ELECTRIC CONDUCTIVITY, σ
Ni-YSZ	-	$400 - 1000\ S \cdot m^{-1}$
LSM	-	$6 - 60\ S \cdot m^{-1}$
YSZ	$180\ S \cdot m^{-1}$	$10 - 15\ S \cdot m^{-1}$

Table 3.2. Conductivity of material used in SOFC

In order to perform a conservative evaluation of the performances of the system, the conductivity values chosen are the lowest ones.

From the constructive and fuel cell design view point, the following considerations can be made to characterise the fuel cell:

- Morphologic, electrical and thermochemical characteristics of materials are uniform and isotropic;
- Electrolyte layer is completely dense.

Then, from the operating point of view, in the first part of the analysis, it is assumed that the syngas is already available and directly injected inside the cell, to avoid temporarily the consideration of the gasification process and to start from a simpler case study. Some further hypotheses are assumed related to the cell operation:

- Fuel cell is working in steady state, isothermal conditions; operating temperature is T=800°C;
- Reactant gas mixtures flowing inside the cell are approximated as ideal gases;
- Laminar gas flows in the channels;
- Electrochemical reactions occur in the thin active layer between the electrolyte and the porous electrode.

Finally, the inlet and outlet boundaries are defined for both anode and cathode channels: on the 2D axisymmetric geometry the inlets and outlets are defined as shown in Figure 3.4 and Figure 3.5.

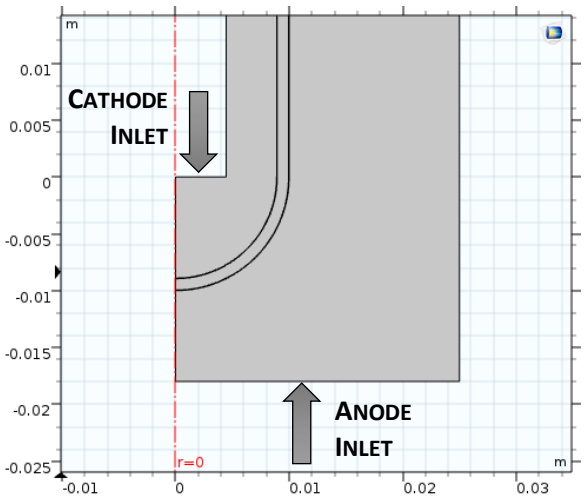

Figure 3.4. Inlet fluxes for both cathode and anode sides

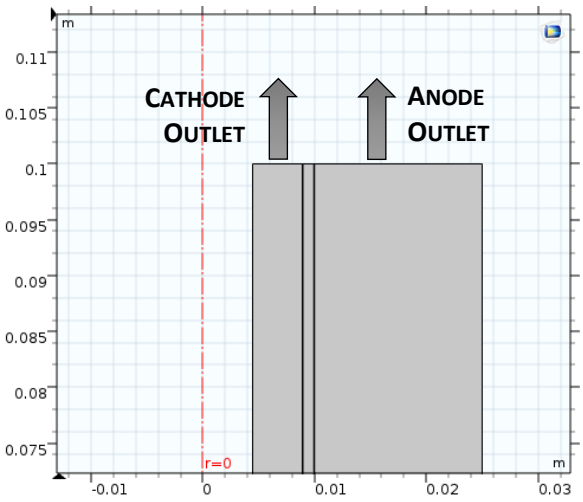

Figure 3.5. Outlet fluxes for both cathode and anode sides

The reactants considered are air for the cathodic side and syngas for the anodic one. The syngas composition is obtained from the previous analysis of the gasification process, considering a content of steam equal to 10% in weight. For the choice of the velocity values, they have been evaluated searching the molar flux needed to obtain 8W of electrical power, assuming a voltage of 0.7V. The Air and Fuel Utilization (AU and FU) has been calculated consequently, to make an evaluation about the exploitation of the inlet flow. The compositions and the velocity values for the nominal case are summed in Table 3.3.

Electrode	**Cathode**	**Anode**
Substance	Air	Syngas
Molar composition	79% N_2 21% O_2	45.44% CO_2 35.08% CO 18.42% H_2O 0.98% H_2 0.08% CH_4
Inlet velocity	0.4 m/s	0.05 m/s
Inlet temperature	800°C	800°C

Table 3.3. Main parameters regarding inlet fluxes

The assumption of laminar flow can be verified evaluating the value of the Reynolds numbers both for air and fuel flows. Knowing that the Reynolds number is equal to:

$$Re = \frac{\rho u d_h}{\mu}$$

where $\rho\ [kg/m^3]$ is the fluid density, $u\ [m/s]$ is the velocity, $d_h\ [m]$ is the characteristic length (in the case of flow inside a tubular duct is represented by the diameter of the tube) and $\mu\ [Pa \cdot s]$ is the dynamic viscosity, it is possible to calculate Re for the air and the syngas flows:

$$Re_{air} = \frac{0.32040 \cdot 0.4 \cdot 0.01}{4.3486 \cdot 10^{-5}} \cong 29.5$$

$$Re_{syngas} = \frac{0.37402 \cdot 0.05 \cdot 0.05}{4.0648 \cdot 10^{-5}} \cong 23.0$$

Those values are very low and well below the threshold levels for laminar regime for flow inside a cylinder (the inlet of both flows, Re<2300). Therefore, the assumption that has been made is coherent with the configuration.

3.2. Polarization curve

As already analysed, the polarization curve describes the variation of the voltage at the terminals of the fuel cell as a function of the current density. When the current density is zero, the cell potential has the highest value, the open-circuit voltage. As the current density increases, the cell potential decreases and can be obtained subtracting to the OCV the various overpotential losses.

The equation that describes this dependence is shown again and is the following:

$$V_{cell} = E_{Nernst} - \eta_{act,an} - \eta_{act,cath} - \eta_{ohm} - \eta_{diff,an} - \eta_{diff,cath} \quad (30)$$

In equation (30), that was already presented in the previous chapter, the fictitious terms of concentration overvoltages appear and the OCV therefore is evaluated considering the partial pressure of species at bulk conditions, since in a mathematical model it could be not trivial the evaluation of gases partial pressure at the point of the reaction. Here the evaluation of the partial pressure at the reaction point is performed by the software. The equation therefore reduces to:

$$V_{cell} = E_{Nernst} - \eta_{act,an} - \eta_{act,cath} - \eta_{ohm} \quad (31)$$

For the evaluation of those contributions, correlations found in literature are used. The OCV terms are taken from the description proposed by Ni [22], the correlations useful for the activation overvoltages evaluation for H_2 and CO are taken from Zhu et al. [21] and A. Leonide et al. [23] respectively.

3.2.1. Nernstian voltage

The first contribution of equation (31) is the Nernstian term. It is calculated starting from the equation already seen in previous sections, here retabled for a better understanding:

$$E_{Nernst} = -\frac{\Delta \bar{g}_{react}(T, p_0)}{z_f \cdot F} + \frac{\bar{R} \cdot T}{z_f \cdot F} \cdot \ln\left(\frac{\prod_1^n \left(\frac{p_i}{p_0}\right)^{\nu_i}}{\prod_1^m \left(\frac{p_i}{p_0}\right)^{\nu_i}}\right) \quad (32)$$

To explicit the dependence of the Nernstian voltage on the temperature and partial pressures of gas species, evaluated at the TPB region, considering the reaction of H_2 it can be written:

$$E_{H_2} = 1.253 - 0.00024516 \cdot T + \frac{\bar{R}T}{2F} \cdot \ln\left[\frac{P_{H_2}\left(P_{O_2}\right)^{0.5}}{P_{H_2O}}\right] \quad (33)$$

In the case of CO electrochemical reaction, the equation is:

$$E_{CO} = 1.46713 - 0.0004527 \cdot T + \frac{\bar{R}T}{2F} \cdot \ln\left[\frac{P_{CO}\left(P_{O_2}\right)^{0.5}}{P_{CO_2}}\right] \quad (34)$$

The working temperature is assumed to be 800°C.

3.2.2. Activation overvoltages

Concerning the activation overvoltages, for both H_2 and CO electrochemical reactions, the kinetic equation is introduced inside the exchange current density i_0 term. The exchange current density is defined for both anodic and cathodic semi-reactions. Moreover, the electrochemical reactions are supposed to occur only in the thin layer located between the electrode gas diffusion layer and the solid electrolyte: it is the catalyst layer, composed by nickel only.

The anodic semi-reaction for hydrogen is the following:

$$H_2 + O^{2-} \rightarrow H_2O + 2\,e^- \quad (35)$$

For the understanding of the process and the following evaluation of the current density, it could be useful to split the oxidation reaction of hydrogen into elementary steps. The reactions mechanism proposed provides for five elementary reactions in the Ni-YSZ three phase zone, that are able to describe the full process. These elementary reactions are defined in Table 3.4.

Adsorption/desorption of H_2 on Ni surface
$H_2(g) + 2(Ni) \leftrightarrow 2H(Ni)$
Charge-transfer at the TPB region
$H(Ni) + O^{2-}(YSZ) \leftrightarrow (Ni) + OH^-(YSZ) + e^-(Ni)$
$H(Ni) + OH^-(YSZ) \leftrightarrow (Ni) + H_2O(YSZ) + e^-(Ni)$
Adsorption/desorption of H_2O on YSZ surface
$H_2O(YSZ) \leftrightarrow H_2O(g) + (YSZ)$
Transfer of O^{2-} in YSZ
$O_0^x(YSZ) + (YSZ) \leftrightarrow O^{2-}(YSZ) + V_0^-(YSZ)$

Table 3.4. Elementary steps of H2 electrochemical oxidation semi-reaction according to [21]

In these equations, on the nickel anode surface, H(Ni) is the adsorbed atomic hydrogen, (Ni) is an empty site, and e^-(Ni) is an electron inside the anode. Concerning the YSZ electrolyte, O^x_o(YSZ) is a lattice oxygen and V^-_o(YSZ) an oxygen vacancy; on the YSZ surface, there can be O^{2-}(YSZ), OH^-(YSZ), H_2O(YSZ) and (YSZ), an empty site. The first reaction involving the OH^- ion is assumed to be the rate determining step. The equation proposed for the evaluation of the exchange current density is:

$$i_0^{H_2} = i^*_{H_2} \cdot \frac{\left(\frac{P_{H_2}}{P^*_{H_2}}\right)^{1/4} \cdot \left(P_{H_2O}\right)^{3/4}}{1 + \left(\frac{P_{H_2}}{P^*_{H_2}}\right)^{1/2}} \quad (36)$$

$$P^*_{H2} = \frac{A_{des}\Gamma^2\sqrt{2\pi RTM_{H_2}}}{\gamma_0} \cdot \exp\left(-\frac{E^{H_2}_{des}}{RT}\right) \quad (37)$$

All the partial pressures appearing in (36) and in the following equations are evaluated in atmospheres. The kinetic parameters shown in the two equations are assumed to be constant and are listed in Table 3.5.

Electro-oxidation of H_2	
Parameter	**Value**
$i^*_{H_2}$	8.5 A/cm^2
A_{des}	5.59 ·10^{19} cm^2/(mol·s)
Γ	2.6·10^{-9} mol/cm^2
γ_0	0.01
$E^{H_2}_{des}$	88 kJ/mol
$\alpha^{H_2}_{a,an}$	1.5
$\alpha^{H_2}_{c,an}$	0.5

Table 3.5. Kinetic parameters for electro-oxidation of H_2

Considering the electrochemical reaction of CO, whose kinetic parameters are listed in Table 3.6, a semi empirical power law model has been applied, to describe the following reaction:

$$CO + O^{2-} \rightarrow CO_2 + 2\,e^- \quad \textbf{(38)}$$

In this case the exchange current density is found as:

$$i_0^{CO} = i^*_{CO} \cdot \exp\left(-\frac{E^{CO}_{act}}{RT}\right) \cdot P_{CO}^{-0.058} P_{CO_2}^{1/4} \quad \textbf{(39)}$$

Electro-oxidation of CO	
Parameter	**Value**
i^*_{CO}	4.56 ·10^6 ·T A/m^2
E^{CO}_{act}	118 kJ/mol
$\alpha^{CO}_{a,an}$	0.62
$\alpha^{CO}_{c,an}$	0.38

Table 3.6. Kinetic parameters for electro-oxidation of CO

On the other electrode, the semi-reaction of the electrochemical reduction of oxygen is:

$$\frac{1}{2}O_2 + 2e^- \rightarrow O^{2-} \quad \textbf{(40)}$$

This reaction can be considered as the result of two elementary steps, as shown in Table 3.7. Here the O_{ads}(c) is the adsorbed atomic oxygen on the cathode surface and (c) is an empty site, while $V^{\cdot}_{o}$(el) and O^{x}_{o}(el) are the oxygen vacancies and lattice oxygen ions in the electrolyte layer; e^{-}(c) is the electron inside the cathode.

Adsorption/desorption of O_2 on LSM surface
$O_2(g) + 2(c) \leftrightarrow 2O_{ads}(c)$
Charge-transfer and adsorption at the TPB region
$O_{ads}(c) + V_0^{\cdot\cdot}(el) + 2e^{-}(c) \leftrightarrow O_0^{x}(el) + (c)$

Table 3.7. Elementary steps of O_2 electrochemical reduction semi-reaction according to [21]

Here the rate limiting step is the charge transfer reaction, and the exchange current density for the cathodic semi-reaction is:

$$i_0 = i^*_{O_2} \frac{\left(\frac{P_{O_2}}{P^*_{O_2}}\right)^{1/4}}{1 + \left(\frac{P_{O_2}}{P^*_{O_2}}\right)^{1/2}} \quad (41)$$

$$P^*_{O_2} = A_{O_2} \exp\left(-\frac{E_{O_2}}{RT}\right) \quad (42)$$

Constant kinetic parameters are shown in the Table 3.8.

Electro-reduction of O_2	
Parameter	**Value**
$\boldsymbol{i^*_{O_2}}$	2.8 A/cm^2
$\boldsymbol{A_{O_2}}$	4.8 ·10^9 atm
$\boldsymbol{E^{O_2}_{act}}$	200 kJ/mol
$\boldsymbol{\alpha_{a,cath}}$	0.5
$\boldsymbol{\alpha_{c,cath}}$	0.5

Table 3.8. Kinetic parameters for electro-reduction of O_2

Then the activation overvoltage is evaluated both at the anode and at the cathode side. At the anode side the linearized Butler-Volmer equation has been used, in the form of:

$$i_{loc} = i_0 \left(\frac{(\alpha_a + \alpha_c) \cdot F}{RT} \right) \eta \quad (43)$$

where i_{loc} is the local current source in [A/m^2] η is the activation overvoltage, and α_a and α_a are the anodic and cathodic transfer coefficient respectively, for the electrochemical oxidation reactions. From literature the following values have been found for the H_2 and CO reactions:

$$\alpha_{a,an}^{H_2} = 1.5 \qquad \alpha_{c,an}^{H_2} = 0.5 \quad (44)$$

$$\alpha_{a,an}^{CO} = 0.62 \qquad \alpha_{c,an}^{CO} = 0.38 \quad (45)$$

While at the cathode side, the cathodic Tafel equation has been applied:

$$i_{loc} = -i_0 \cdot 10^{\frac{\eta}{A_c}} \quad (46)$$

in which A_c is the cathodic Tafel slope, evaluated as $-(RT)/(z_{fuel}\alpha F)$. In the case of the electrochemical reduction of oxygen, transfer coefficients are equal:

$$\alpha_{a,cath} = 0.5 \qquad \alpha_{c,cath} = 0.5 \quad (47)$$

The linearized Butler-Volmer equation has been preferred to the not linear one with the aim of reducing the computational efforts. On the other hand, the Tafel equation has been applied at the cathodic side: the high values of overvoltages that can be reached at the cathode side justify this choice, since this equation replace the Butler-Volmer one in case of high values of η.

3.2.3. Ohmic overvoltages

The last contribution of equation (31) to be defined is the ohmic losses term. The ohmic overpotential is mainly due to the electrolyte resistance to the O^{2-} ions transport, and it is simply evaluated with Ohm's law:

$$\eta_{ohm} = iL\frac{1}{\sigma} \quad (48)$$

in which L is the thickness of the electrolyte and σ is the ionic conductivity of the electrolyte, espressed in [$\Omega^{-1}m^{-1}$].

3.3. Diffusion model

From the previous equations it can be noticed that the SOFC model aims to evaluate the voltage at the terminals of the cell as function of some independent parameters, such as pressure, temperature, current density and reactants compositions. In particular, if fixed

thermodynamic conditions are assumed, the cell voltage becomes a function of the current flowing inside the cell and the gases compositions. It is therefore necessary to apply suitable equations to model the diffusion of gases inside the electrodes.

The diffusion process inside a pore can be subdivided into two mechanisms, molecular diffusion and Knudsen diffusion. Molecular diffusion is the dominant phenomenon in case of large pore size and high pressures, while Knudsen diffusion contribution increase when the mean-free path of molecules is much higher than the pore size.

As anticipated previously, the Fick's law is used to describe the motion of gaseous fluid mixtures through the porous structure of electrodes. In reality, the most accurate model for this kind of simulation would be the Dusty Gas one. The main hypothesis assumed, that would make it particularly appropriate for this study, is that if a system of *n* gaseous species is considered flowing though the porous medium, the porous medium itself is considered as the (*n*+1)-th component of the mixture, composed by big molecules (the dust particles) forced to remain in a fixed position by a virtual external force. Comsol, however, does not include the Dusty Gas among the possible diffusion models; Fick and Stefan-Maxwell models are instead available. Since Maxwell-Stefan model does not allow to consider the Knudsen diffusion mechanism, Fick's law has been considered the better solution.

The general equation describing the diffusion phenomenon according to Fick's law implemented in the software is the following:

$$\boldsymbol{j}_i = -\left(\rho D_i^{fK} \nabla w_i + \rho w D_i^{fK} \frac{\nabla M_n}{M_n} + D_i^T \frac{\nabla T}{T}\right) \quad (49)$$

where:

- $\boldsymbol{j}_i \left[\frac{kg}{m^2 s}\right]$ is the diffusion flux of the specific substance *i*;
- $\rho \left[\frac{kg}{m^3}\right]$ is the density of the mixture;
- $D_i^{fK} \left[\frac{m^2}{s}\right]$ is the diffusion coefficient or diffusivity, in which both the molecular diffusion (indicated with the apex *f*) and the Knudsen effect (*K*);
- $w_i \left[\frac{kg_i}{kg}\right]$ is the mass fraction of gas *i*;
- $M_n = \left(\sum_i \frac{w_i}{M_i}\right)^{-1} \left[\frac{kg}{mol}\right]$ is the molar mass of the mixture;
- $D_i^T \left[\frac{kg}{ms}\right]$ is the thermal diffusion coefficient, that in this work has not been considered for simplicity.

The main aspect is the evaluation of the diffusion coefficient, that correlates the two terms of diffusion in the following way:

$$D_i^{fK} = \left(\frac{1}{D_{ij}^f} + \frac{1}{D_i^K} \right)^{-1} \quad (50)$$

The first contribution of binary diffusion coefficient is evaluated according to the equation:

$$D_{ij}^f = \frac{0.00266\, P_{atm} T^{3/2}}{0.01^2\, P\, \Omega_{D,ij}\, \tilde{\sigma}_{ij}^2\, M_{ij}^{1/2}} \quad (51)$$

The second term of equation (50) represents the Knudsen diffusion coefficient, whose value is calculated with:

$$D_i^K = \frac{\lambda_{path}}{3} \sqrt{\frac{8RT}{\pi M_i}} \cong 97.0 \frac{d_{pore}}{2} \sqrt{\frac{T}{M_i}} \quad (52)$$

in which the $\lambda_{path}\ [m]$ is the mean free path of the molecules of gases and $d_{pore}\ [m]$ is the pore diameter.

The parameters shown in equations (51) and (52) are listed in Table 3.9.

Parameter	Unit of measure	Espression/Value
$\boldsymbol{\Omega_{D,ij}}$	[-]	$\frac{A}{(T_{ij}^*)^B} + \frac{C}{\exp(DT_{ij}^*)} + \frac{E}{\exp(FT_{ij}^*)} + \frac{G}{\exp(HT_{ij}^*)}$ $T_{ij}^* = kT/\epsilon_{ij}$ $A = 1.06036$ $B = 0.15610$ $C = 0.19300$ $D = 0.47635$ $E = 1.03587$ $F = 1.52996$ $G = 1.76474$ $H = 3.89411$
$\boldsymbol{\epsilon_{ij}}$	[J]	$\sqrt{\epsilon_i \cdot \epsilon_j}$
$\boldsymbol{k}$	[J/K]	$1.38065 \cdot 10^{-23}$
$\boldsymbol{\tilde{\sigma}_{ij}}$	[Å]	$\frac{\sigma_i + \sigma_j}{2}$
$\boldsymbol{M_{ij}}$	[kg/kmol]	$2\left(\frac{1}{M_i} + \frac{1}{M_j}\right)^{-1}$
$\boldsymbol{d_{pore}}$	[m]	$1.1 \cdot 10^{-6}$

Table 3.9. Parameters used for diffusion equations according to [24]

When the diffusion inside the porous structure is considered, the molecular diffusion coefficient can be adjusted according to the tortuosity model: in such way, the term of diffusion becomes:

$$D_i^{fK} = \left(\frac{1}{D_{ij}^{eff,f}} + \frac{1}{D_i^K} \right)^{-1} \quad (53)$$

with

$$D_i^{eff,f} = \frac{\epsilon_p}{\tau_f} D_i^f \quad (54)$$

where $D_i^{eff,f}$ is the effective molecular diffusivity and:

- ϵ_p $[-]$ is the porosity of the material;
- τ_f $[-]$ is the tortuosity of the fluid inside the porous medium.

Besides this, in case of occurrence of heterogenous chemical reactions, the reactions stoichiometry has to be considered, since it can change the composition of the mixture. While for the cathode side this is not an issue, since there is no heterogeneous reaction that can consume oxygen, this phenomenon has to be taken into account at the anode side, where steam methane reforming and water gas shift reactions can occur. Therefore, in the balance equation:

$$\nabla \cdot \boldsymbol{j}_i + \rho(\boldsymbol{u} \cdot \nabla) w_i = R_i \quad (55)$$

the term R_i $\left[\frac{kg}{m^3 s}\right]$ is the source term, in which the rate of reactions is considered.

3.4. Heterogeneous reactions model

Since in diffusion equations, the source term R_i related to the occurrence of side reactions in the electrode region is present, a model is necessary to evaluate this contribution. The two main reactions considered are the water gas shift and the methane steam reforming, which are able to change the syngas composition and the H_2/CO ratio. These reactions are defined heterogeneous, since they occur in (and may be catalysed by) the porous material constituting the electrode, differently from the homogeneous reactions, which occur only in the gas phase. The correlations used to define the reaction kinetics are the ones proposed by the study of Haberman and Young, which have been widely used, and then adopted by M. Ni [25]; additionally, the rate data used in this study are referring to an anode electrode made of Ni-YSZ, therefore it is particularly appropriate for this work.

The two reactions are re-written below, the water gas shift:

$$CO + H_2O \xrightarrow{k_{sf}} H_2 + CO_2 \quad (56)$$

and the steam methane reforming:

$$CH_4 + H_2O \xrightarrow{k_{rf}} 3H_2 + CO \quad (57)$$

where k_{sf} and k_{rf} are the forward reaction rate constants of the catalysed reactions. These two terms [mol m^{-3} Pa^{-2} s^{-1}] are defined according to the Arrhenius formula:

$$k_{sf} = 0.0171 \exp\left(-\frac{103191}{RT}\right) \quad (58)$$

$$k_{rf} = 2395 \exp\left(-\frac{231266}{RT}\right) \quad (59)$$

while the equilibrium constants K_{ps} and K_{pr} are defined according to the following empirical correlations, functions of temperature:

$$K_{ps} = \exp(-0.2935\, Z^3 + 0.6351\, Z^2 + 4.1788\, Z + 0.3169) \quad (60)$$

$$K_{pr} = P_{atm}^2 \exp(-0.2513\, Z^4 + 0.3665\, Z^3 + 0.5810\, Z^2 - 27.134\, Z + 3.2770) \quad (61)$$

with $Z = \frac{1000}{T[K]} - 1$ as dimensionless term.

Exploiting these parameters, it is possible to evaluate the rate [mol/(m^3·s)] of SMR and WGS reactions:

$$R_{WGS} = k_{sf}\left(p_{CO}p_{H_2O} - \frac{p_{CO_2}p_{H_2}}{K_{ps}}\right) \quad (62)$$

$$R_{SMR} = k_{rf}\left(p_{CH_4}p_{H_2O} - \frac{p_{CO}p_{H_2}^3}{K_{pr}}\right) \quad (63)$$

From these expressions, a balance for each chemical species present in gas mixture can be applied and inserted in the equation (64), according to the stoichiometry of the two reactions:

$$R_i = \left(\nu_{i,WGS}R_{WGS} + \nu_{i,SMR}R_{SMR}\right) \cdot M_i \quad (64)$$

and in particular for the species present:

$$R_{H_2} = (R_{WGS} + 3\, R_{SMR}) \cdot M_{H_2} \quad (65)$$

$$R_{H_2O} = (-R_{WGS} - R_{SMR}) \cdot M_{H_2O} \quad (66)$$

$$R_{CO} = (-R_{WGS} + R_{SMR}) \cdot M_{CO} \quad (67)$$

$$R_{CO_2} = (R_{WGS}) \cdot M_{CO_2} \quad (68)$$

$$R_{CH_4} = (-R_{SMR}) \cdot M_{CH_4} \quad (69)$$

where the molecular weight M_i is added to obtain the correct unit of measure.

With the application of the latter equations, the kinetics of the reactions is totally defined. To further describe the phenomena occurring inside the control volume and to fully describe the SOFC operation, if fed with syngas directly, the last term that can be introduced is the heat generation inside the fuel cell.

3.5. Heat generation model

This part of the simulation can be useful to analyse the source of losses inside the fuel cell and the temperature gradients that can arise, that could lead to the generation of thermo-mechanical stresses inside the materials. Two main sources of heat can be considered:

- The heat generated as a result of the fuel cell operation, due to the activation, ohmic and concentration overpotentials;
- The heat generated as a result of the occurrence of the electrochemical and chemical reactions, related to the exothermicity or exothermicity of the reactions.

The first kind of source is already implemented on the software, under the name Total power dissipation density [W/m^3]. The second source of heat is introduced using relation found from literature. The reactions that are considered are the electrochemical reactions of H_2 and CO, that are both exothermic, and the WGS and SMR chemical reactions, which are the first exothermic and the second one endothermic.

The heat generated due to the occurrence of the electrochemical reactions can be estimated by applying the second law of thermodynamics and therefore it will be:

$$\Phi_1 = (\Delta \bar{s}_{react} T) \cdot \dot{n}_{fuel} = \frac{\Delta \bar{s}_{react} T}{z_{fuel} F} \cdot I_{vol} \quad (70)$$

In this equation, the term of current appearing I_{vol} is a volumetric current expressed as [A/m^3] and is evaluated by the software.

Considering the electrochemical reaction of hydrogen, the associated molar entropy variation is evaluated as:

$$\Delta \bar{s}_{H_2} = \bar{s}_{H_2O} - \bar{s}_{H_2} - \frac{1}{2} \bar{s}_{O_2} \quad (71)$$

according to the stoichiometric coefficients. The values of entropy are evaluated using empiric relations as functions of temperature.

The same kind of equation can be applied to the electrochemical reaction involving carbon monoxide, in which each value of entropy is evaluated in a similar way as for hydrogen:

$$\Delta\bar{s}_{CO} = \bar{s}_{CO_2} - \bar{s}_{CO} - \frac{1}{2}\bar{s}_{O_2} \quad (72)$$

The values of entropy for each substance, evaluated at a temperature of 800°C and a pressure of 1atm is shown in Table 3.10.

Compound	Entropy (T=800°C, p=1 atm) [J/(mol·K)]
H_2	167.54
H_2O	172.18
CO	236.16
CO_2	272.48
O_2	245.79

Table 3.10. Entropy at T=800°C and p=1 atm of the analysed compounds

The reaction heat for the WGS and SMR is evaluated using the following equations [25]:

$$H_{WGS} = 45063 - 10.28 \cdot T \quad (73)$$

$$H_{SMR} = -(206205.5 + 19.5175 \cdot T) \quad (74)$$

where both equations give as a result a value in [J/mol]. To obtain the heat in the correct unit of measure [W/m^3], the H_{WGS} and H_{SMR} have to be multiplied by the reaction rates in [mol/(m^3·s)] previously obtained, that are R_{WGS} and R_{SMR} respectively:

$$\Phi_2 = H_{WGS} \cdot R_{WGS} + H_{SMR} \cdot R_{SMR} \quad (75)$$

Considering all these contributions, an analysis on the thermal generation and the subsequent heat transfer can be performed, obtaining the distribution of temperature inside the fuel cell.

3.6. Gasification model

The evaluations made so far have been made considering the direct injection inside the fuel cell of already produced syngas; the gasification process was therefore not present. Now this process is analysed to perform such simulation.

To simulate the gasification process, it is necessary to apply the equations of mass conservation for the solid and gaseous species. In most of case studies proposed on literature, the works are focused either on the first pyrolysis step or on the char gasification, the second step. To consider the whole process, the relations proposed in the thesis of C. Guizani [26] are considered. Additionally, since an experimental phase to obtain empirical values specific for the olive kernel biomass has not been possible, the data proposed by Guizani for the data related to the biomass are used.

The gasification is studied as a sequence of reactions that lead to the formation of the final products CO, CO_2, H_2, H_2O and CH_4 from the original biomass matter. The work carried out by Guizani proposes the following steps to describe the gasification process:

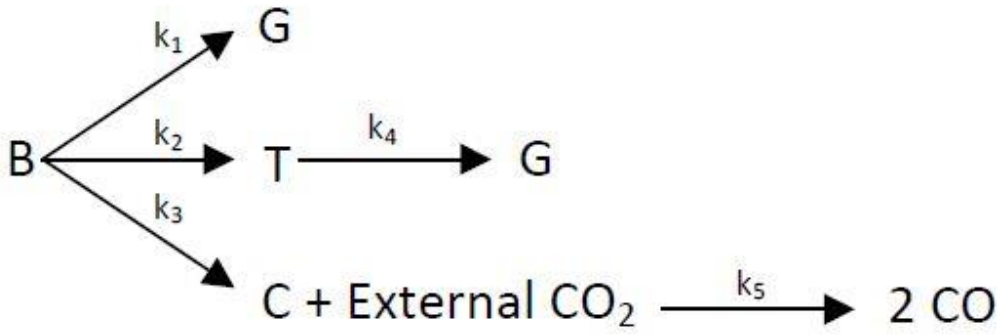

Figure 3.6. Reactions involved in the pyro-gasification process [26]

In Figure 3.6, the reactions constituting the pyro-gasification process are shown. The process is represented with three parallel reactions which describe the decomposition of the initial biomass matter (B) into pyrolysis gas (G, reaction R1), tars (T, reaction R2) and char (C, reaction R3). The secondary reactions R4 and R5 define the tar cracking process and the char gasification respectively: the latter reaction between char and the surrounding CO_2 is represented in the form of the Boudouard reaction.

In order to try to simplify the complex phenomenon, some hypotheses are considered:

- Biomass density has been obtained from literature;
- Reactions follow Arrhenius law;
- Char is assumed to be composed only by carbon;
- Gaseous species diffuse according to Fick's law.

In order to simplify the further analysis, also the biomass matter will be considered as composed by carbon only.

In particular, for the gaseous species, the following hypotheses introduced by Guizani are considered:

- CO_2, which is the gasifying agent, is supposed to be initially present in the surrounding of the SOFC;
- Gases, emitted by the biomass decomposition, have an average molecular value of 22 g/mol;
- Tars are assumed to have a molecular weight of 78 g/mol.

In the light of such simplifying assumptions, the mass conservation equations have been applied for both solid and gaseous species.

The decomposition of biomass is described as:

$$\frac{\partial \rho_B}{\partial t} = -(w_G k_1 + w_T k_2 + w_C k_3)\rho_B \quad (76)$$

while the char formation and the following gasification is described by the equation:

$$\frac{\partial \rho_C}{\partial t} = w_C k_3 \rho_B - k_5 \rho_C P_{CO_2} \quad (77)$$

Since in this work a stationary configuration is considered, a source term for the biomass is needed, to take into account the continuous introduction of primary source into the reactor, considering a biomass feeding rate of around 15kg/h for the total reactor (that corresponds roughly to 0.6kg/h for each fuel cell control volume).

For the mass conservation applied to the gaseous species, four additional equations are necessary. The CO_2 conservation equation is described as:

$$\frac{\partial \epsilon \rho_{CO_2}}{\partial t} + \nabla \cdot \left(\rho_{CO_2} u - D_{eff} \nabla \rho_{CO_2}\right) = -k_5 \rho_C P_{CO_2} \quad (78)$$

The CO conservation equation is described as:

$$\frac{\partial \epsilon \rho_{CO}}{\partial t} + \nabla \cdot \left(\rho_{CO} u - D_{eff} \nabla \rho_{CO}\right) = +k_5 \rho_C P_{CO_2} \quad (79)$$

The tars conservation equation is described as:

$$\frac{\partial \epsilon \rho_T}{\partial t} + \nabla \cdot \left(\rho_T u - D_{eff} \nabla \rho_T\right) = w_T (k_2 \rho_B - \epsilon k_4 \rho_T) \quad \textbf{(80)}$$

The pyrolysis gas conservation equation is described as:

$$\frac{\partial \epsilon \rho_G}{\partial t} + \nabla \cdot \left(\rho_G u - D_{eff} \nabla \rho_G\right) = w_G k_1 \rho_B + w_T \epsilon k_4 \rho_T \quad \textbf{(81)}$$

In such equations, ϵ $[-]$ is the reactor porosity, that here corresponds to the region surrounding the fuel cell: this is equal to the estimated value of the biomass porosity (in the region where the biomass is supposed to be present), otherwise it is equal 1. Then, the terms w_i $[-]$ are the mass stoichiometric coefficients for char (w_C), gas (w_G) and tars (w_T), that are linked together according to:

$$w_C + w_G + w_T = 1 \quad \textbf{(82)}$$

The yield values affect deeply the results of the gasification, in terms of component concentrations. Since an average composition of the syngas has already been obtained through experimental analysis, to develop a model as representative as possible the final concentrations of the syngas components should be as close as possible to the ones already known. The values of tar and char yield (respectively, 0.05 and 0.12) assumed by Guizani are not suitable for this work, since the gas yield of 0.87 pushes strongly the gasification towards the production of pyrolysis gas that are not present in the previous syngas composition shown in section 2.3.5 (Figure 2.8). Therefore, different values have to be considered. From the study on biomass gasification performed by Chaurasia [27], different values are presented: the tars from pyrolysis undergo secondary cracking, in which stable tars represents the 6% and CH_4 the 10.2%. Since, as it is clarified later, the pyrolysis gas is assumed to be a mixture of methane and ethylene, a value of w_G of about 0.1 can be a good approximation. In this way, it is possible to push the gasification towards the production of CO rather than the production of tars and gases, in order to remain coherent with the previous gasification results. Additionally, the terms k_i $[s^{-1}]$ are the reaction rate constants, evaluated using the Arrhenius law:

$$k_i = A_i \exp\left(-\frac{E_i}{RT}\right) \quad \textbf{(83)}$$

and whose kinetic parameter are summed in Table 3.11.

Reaction rate constant $[s^{-1}]$	Pre-exponential factor, A $[s^{-1}]$	Activation energy, E $[kJ/mol]$
k_1	$1.3 \cdot 10^8$	140
k_2	$2 \cdot 10^8$	133
k_3	$1.08 \cdot 10^7$	121
k_4	$3.2 \cdot 10^4$	72.8
k_5	$1.04 \cdot 10^2$	200

Table 3.11. Kinetic parameters of pyro-gasification reactions

These equations, however, are not sufficient to describe the process that leads to the production of the desired products. Further equations that describe the main reactions between the compounds already present are needed.

Firstly, it is necessary to identify the species constituting the tars and pyrolysis gases. Knowing the values of molar masses, the following choices have been assumed:

- For tars, it has been assumed they are constituted by benzene (C_6H_6) solely, having a molar mass of exactly 78 g/mol;
- For pyrolysis gas, since the value of 22 g/mol does not correspond to any hydrocarbon molecule, a mixture composed by 50 mol% of CH_4 (16 g/mol) and 50 mol% of C_2H_4 (28 g/mol) has been considered, in such a way the resulting molar mass of the mixture will be exactly 22 g/mol.

In this way, knowing the exact composition of the mixture, it is possible to apply to each species the main reactions that could occur in a gasification process, to analyse the final concentrations of the desired products.

The resulting reactions scheme therefore would be the following:

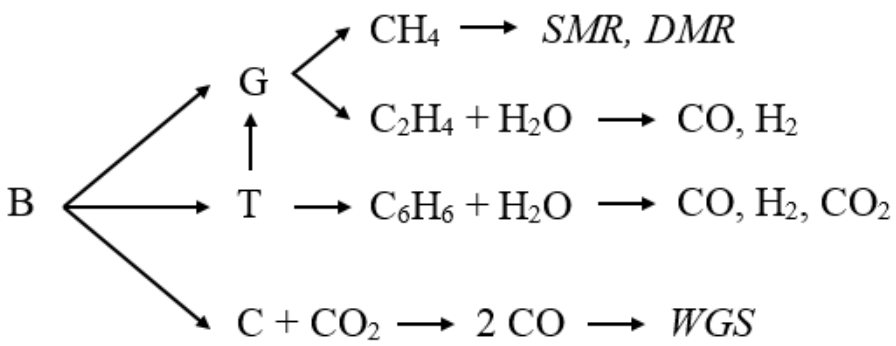

Figure 3.7. Complete scheme of reactions considered for the pyro-gasification model

For the compounds here introduced, that are C_2H_4 and C_6H_6, the reactions with steam are considered (steam reforming reactions of ethylene and benzene). Additionally, the Dry Methane Reforming (DMR) with carbon dioxide is considered, due to the high concentration of CO_2 in this study case. The reaction kinetics are different, and so the modelling equations. The reactions occurring and the respective reaction kinetics are the following:

- Boudouard reaction (whose parameters are already listed):

$$C + CO_2 \rightarrow 2\,CO \quad (84)$$

- Steam methane reforming (R6):

$$CH_4 + H_2O \rightarrow CO + 3\,H_2 \quad (85)$$

- Dry methane reforming (R7):

$$CH_4 + CO_2 \rightarrow 2\,CO + 2\,H_2 \quad (86)$$

- Water gas shift (R8):

$$CO + H_2O \rightarrow CO_2 + H_2 \quad (87)$$

- Steam ethylene reforming (R9):

$$C_2H_4 + 2\,H_2O \rightarrow 2\,CO + 4\,H_2 \quad (88)$$

- Steam benzene reforming (R10, R11):

$$C_6H_6 + 12\,H_2O \rightarrow 6\,CO_2 + 15\,H_2 \quad (89)$$

$$C_6H_6 + 6\,H_2O \rightarrow 6\,CO_2 + 9\,H_2 \quad (90)$$

These reactions follow equations of various behaviours, according to the different formulations proposed in literature. Reactions R6 and R8 and their parameters have been already described in section 3.4, the others are showed below.

The Dry Methane Reforming (R7) is modelled according to the relation used by Lee et al. [28] shown below:

$$R7 = k_7 \cdot \left[\frac{K_{CO_2}K_{CH_4}P_{CO_2}P_{CH_4}}{\left(1 + K_{CO_2}P_{CO_2} + K_{CH_4}P_{CH_4}\right)^2}\right] \cdot \left[1 - \frac{\left(P_{CO}P_{H_2}\right)^2}{K_1 P_{CH_4} P_{CO_2}}\right] \quad (91)$$

where:

$$K_{CO_2} = 2.64 \cdot 10^{-2} \cdot \exp\left(\frac{37641\left[\frac{J}{mol}\right]}{RT}\right)\left[\frac{1}{atm}\right] \quad (92)$$

$$K_{CH_4} = 2.63 \cdot 10^{-2} \cdot \exp\left(\frac{40684\left[\frac{J}{mol}\right]}{RT}\right)\left[\frac{1}{atm}\right] \quad (93)$$

$$k_7 = 1290 \cdot 5000 \cdot \exp\left(-\frac{102065\left[\frac{J}{mol}\right]}{RT}\right)\left[\frac{mol}{s \cdot m^3}\right] \quad (94)$$

$$K_1 = \exp(34.011) \cdot \exp\left(-\frac{258598\left[\frac{J}{mol}\right]}{RT}\right)\left[atm^2\right] \quad (95)$$

The Steam Ethylene Reforming (R9) kinetics is obtained from the study of Abdalla et al. [29], whose relation is described as:

$$R9 = k_9 \cdot P_{H_2O} \cdot P_{C_2H_4}^{0.5} \quad (96)$$

where

$$k_9 = \exp\left(0.12 - \frac{103996\left[\frac{J}{mol}\right]}{RT}\right) \quad (97)$$

Finally, the two equations for Steam Benzene Reforming are considered (R10 and R11), obtained from Ammar et al. [30], in the form:

$$R10 = k_{10} \cdot c_{C_6H_6} \cdot c_{H_2O} \quad (98)$$

$$R11 = k_{11} \cdot c_{C_6H_6} \cdot c_{H_2O} \quad (99)$$

where:

$$k_{10} = 70.858 \cdot \exp\left(-\frac{462.803\left[\frac{kJ}{mol}\right]}{RT}\right) \quad (100)$$

$$k_{11} = 394.817 \cdot \exp\left(-\frac{1048.977\left[\frac{kJ}{mol}\right]}{RT}\right) \quad (101)$$

Through the application of those equations, the simulation of the complete gasification has been performed, from the degradation of the solid matter to the final producer gas.

Finally, the last part is the description of the heat transfer inside the system. To simplify the estimation, the assumption made is that the heat necessary for the pyro-gasification of the biomass material is completely sustained by an external heat source, and, as for the case of the operation of the fuel cell, the reactions that have been considered are the SMR and WGS.

4. STUDY CASES AND RESULTS

The models used for the simulation of the two main processes have been implemented on COMSOL Multiphysics ® 5.3.

Firstly, the SOFC has been modelled: the operation of such fuel cell has been analysed, comparing different operating conditions. In this way, the gasification process can be temporarily neglected, as the syngas is considered as already produced. The performances of the syngas-fed cell are then compared to the theoretical performances of the cell fed with an equivalent amount of hydrogen, so to produce the same current.

In the second part, the gasification process is analysed, firstly as a single process; finally the coupling with the SOFC operation has been realized, to describe in a more complete way the system.

On COMSOL Multiphysics ® 5.3, the phenomena occurring in the operation of the fuel cell and in the gasification process are simulated through a series of physics. To model the SOFC functioning, three different physics are used:

- *Free and Porous Media Flow* (one for anode and one for cathode sides), to describe the gas flows into the channels and inside the porous structure of electrodes, up to the catalyst layers, and to obtain the velocity field;
- *Transport of Concentrated Species* (one for anode and one for cathode sides), to describe the composition of the flows and to obtain the molar and mass fractions of the components of gas mixtures;
- *Secondary Current Distribution*, to simulate the occurrence of the electrochemical reactions and the subsequent potential difference and then current productions.

These are the fundamental physics necessary to the simulation of the SOFC; however, another aspect to be taken into account is the production of heat, that could lead to the generation of thermal gradients deleterious for the cell. The further physics useful to perform a thermal analysis on the fuel cell is the following:

- *Heat Transfer in Porous Media*, to describe the heat generation inside the cell and to obtain a temperature distribution.

For which concerns the gasification, three physics are necessary:

- *Ordinary Differential Equations*, to apply the mass conservation for the solid-state materials;
- *Transport of Diluted Species*, to apply the mass conservation at the gaseous species, introducing the reactions occurring. The Transport of Diluted Species physics is necessary in this case, rather than the Transport of Concentrated Species, since it is assumed that one gas species (in this case CO_2, the gasifying agent) is present in a much greater amount compared to the others;
- *Heat Transfer in Fluids*, to describe the heat transfer inside the gaseous products of the gasification.

These are the main physics used, through which the following results are obtained. Obviously, the final coupling of the gasification process and SOFC operation will require the simultaneous presence of all the physics listed above (excluding the *Transport of Concentrated Species* for the anode side, that is replaced by the *Transport of Diluted Species*).

4.1. Nominal configuration: SOFC operation with syngas

The project aims at the construction of a stack of 25 cells that could produce a total electric power of about 0.2 kW, that means around 8W per cell; the cells are located at a distance of 5cm between each other.

In the first simulation the cell is made to work in the nominal configuration and design. Due to the complex geometry of the cell and to the absence of an anode channel that could better funnel the fuel inside the porous anode (avoiding fuel dispersion), the inlet velocities needed to achieve the final product are higher than the stoichiometric ones.

The operating conditions are summed in the table below.

Temperature	800°C
Pressure	1atm
Anode inlet velocity	0.05 m/s
Cathode inlet velocity	0.4 m/s

Table 4.1. Main parameters describing the operating conditions

Then the initial conditions are set:

- The initial pressure inside both anode and cathode side is set equal the atmospheric pressure (101325 Pa);
- The operating temperature is set equal to 800°C;
- Inside the channel and the electrodes no initial velocity field is assumed: the velocity fields are estimated thanks to the Free and Porous Media physics.

The mesh is physics-controlled and the tolerance is set at 10^{-3}.

The distribution of velocities is shown in Figure 4.1.

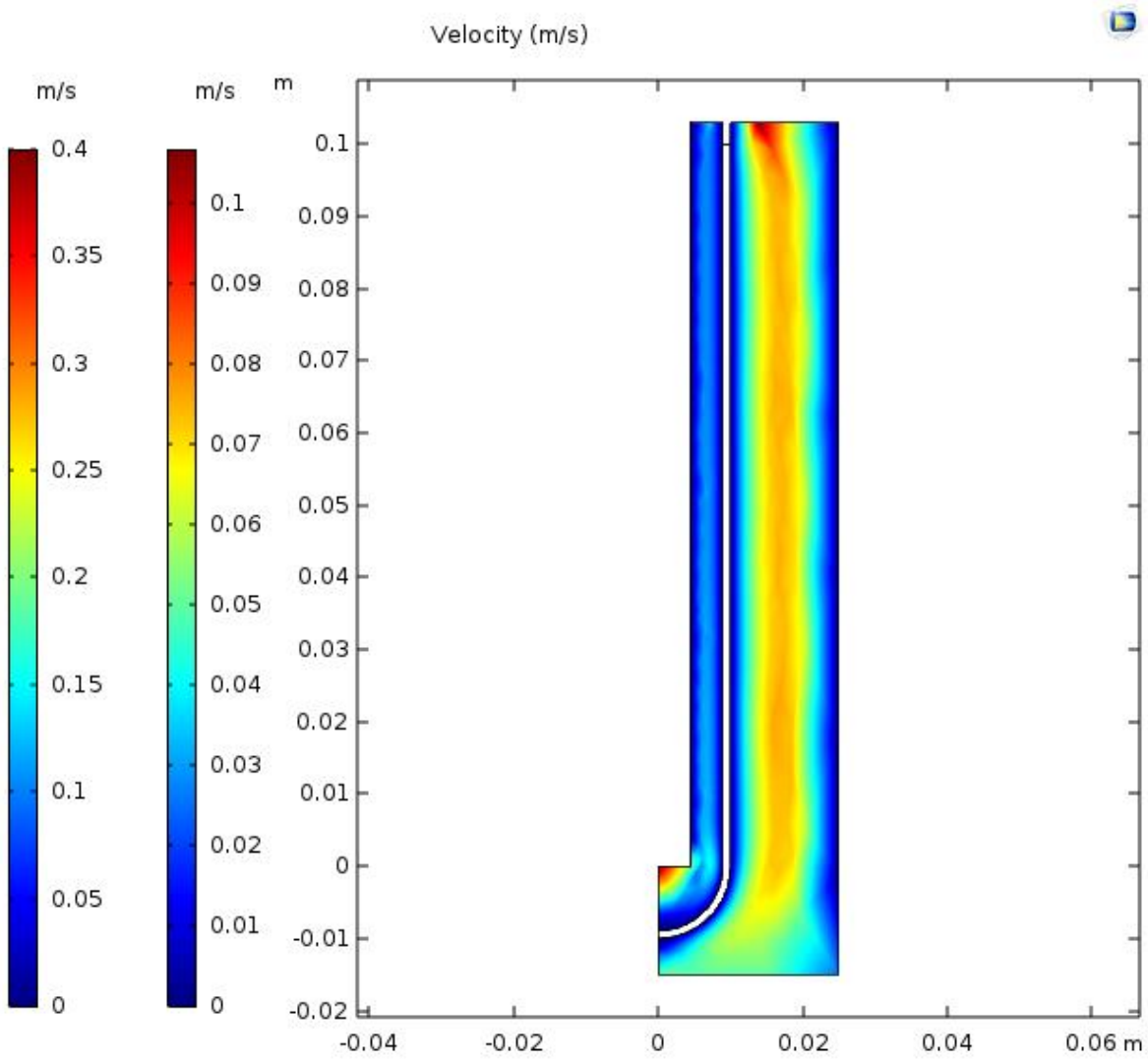

Figure 4.1. Velocity field inside the cell

Observing the velocities distribution, it is clear the impact of the fuel losses at the anode side: the great dimensions of the anode channel do not guarantee a good exploitation of the fuel, that in large part does not reach the anode electrode but simply tends to go towards the outlet, without producing any useful effect.

The polarization curve is shown in Figure 4.2 and the power density curve in Figure 4.3.

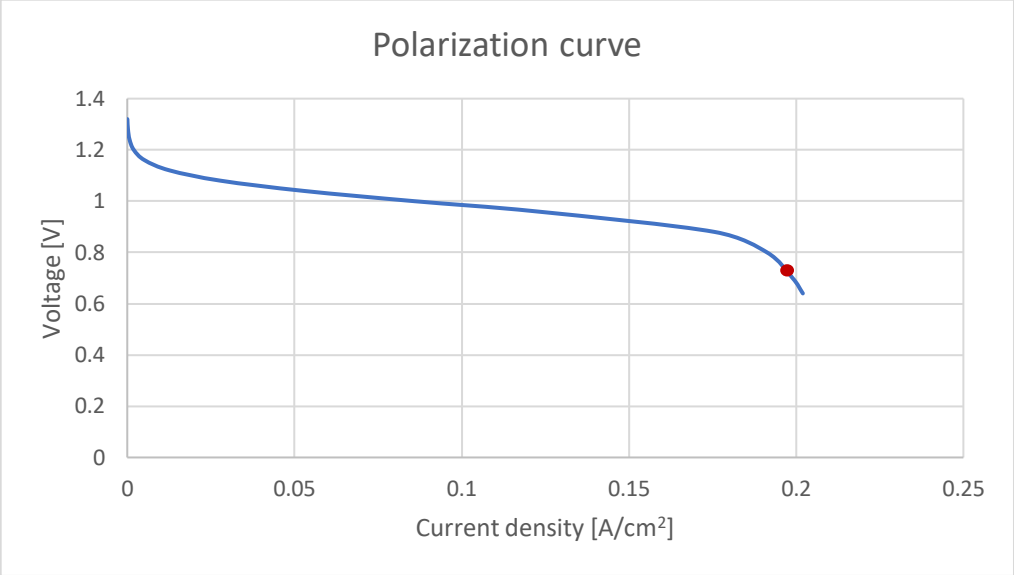

Figure 4.2. Polarization curve of the fuel cell

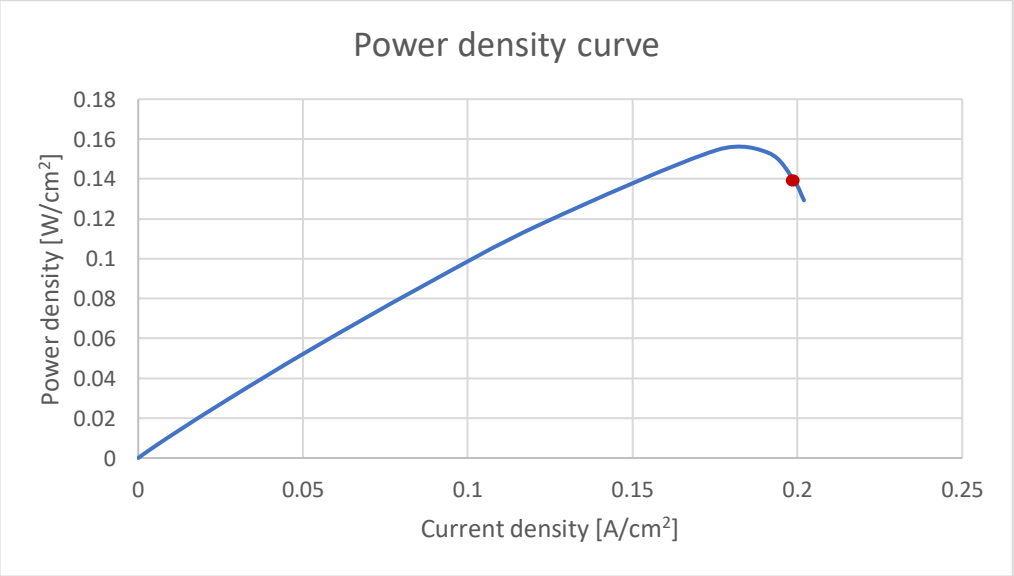

Figure 4.3. Power density curve of the fuel cell

In the graph above, the three regions are well visible on the curve: the first part characterized by the activation overvoltages, the second one (from about 0.03A/cm^2 to 0.17A/cm^2) characterized by the linear behaviour typical of the ohmic region and the third in which the concentration losses are dominating. The operating conditions in which the fuel cell would work (indicated by the red dot in Figure 4.2) are located in the final part of the curve,

where the concentration losses are important. This configuration, even if it allows to reach the required power, could be affected by fuel starvation phenomena.

The current density at the typical voltage of 0.7V is 0.20A/cm^2: this value guarantees the achievement of the 8W of output power, more precisely a power of 9.59W, that is slightly higher. However, this is a conservative evaluation since the model does not takes into account the effect of carbon deposition that, with the time, could reduce the catalyst activity. Anyway, this configuration does not represent an efficient utilization of the SOFC. The evaluation of the fuel utilization and the electrical efficiency is performed as follows:

$$FU = \frac{\dot{n}_{syngas,st}}{\dot{n}_{syngas,real}} \quad (102)$$

$$\eta_{el} = \frac{W_{el}}{\dot{n}_{fuel} \cdot \overline{HHV}} \quad (103)$$

in which $\dot{n}_{syngas,st}$ represents the reacting fraction of syngas, $\dot{n}_{syngas,real}$ the total amount of syngas sent inside the anode channel and $\overline{LHV}$ is the molar low heating value of the fuel contained in the syngas.

The $\overline{HHV}$ $\left[\frac{J}{mol}\right]$ is estimated considering the enthalpy of reactions of the three fuels contained in the syngas:

$$\overline{HHV}_{H_2} = \left|\bar{h}_{H_2O} - \frac{1}{2}\bar{h}_{O_2} - \bar{h}_{H_2}\right| = 241820\frac{J}{mol} \quad (104)$$

$$\overline{HHV}_{CO} = \left|\bar{h}_{CO_2} - \frac{1}{2}\bar{h}_{O_2} - \bar{h}_{CO}\right| = 282990\frac{J}{mol} \quad (105)$$

$$\overline{HHV}_{CH_4} = \left|\bar{h}_{CO_2} + 2\bar{h}_{H_2O} - 2\bar{h}_{O_2} - \bar{h}_{CH_4}\right| = 802310\frac{J}{mol} \quad (106)$$

Then each low eating value is multiplied by the corresponding molar fraction of the fuel to obtain the $\overline{HHV}$ of the syngas.

$$\overline{HHV}_{syngas} = 101633\frac{J}{mol} \quad (107)$$

Considering the values obtained above, the results are not so satisfactory. Actually, the performances of the cell are quite low, being:

$$FU = 17.5\% \quad (108)$$

$$\eta_{el,whole\ syngas} = 8.5\% \quad (109)$$

However, this efficiency takes into account all the fuel sent from the inlet section and it is much different from the amount of fuel that actually enters inside the cell. To have a precise evaluation of the performances of the fuel cell only the syngas that manage to reach the porous

electrode should be taken into account. Therefore, to have a better estimation of the electric efficiency, the previous value of η_{el} could be divided by the value of FU, in order to really estimate the efficiency of conversion of the chemical energy into the electrical energy. The real electrical efficiency therefore become:

$$\eta_{el} = 48.4\% \quad \textbf{(110)}$$

This value is much higher than the previous and is coherent with the typical efficiency values of fuel cells.

Concerning the air utilization (AU), instead, the situation is different. Using a similar formula to the one above used for the fuel utilization, it is possible to obtain:

$$AU = 59.3\% \quad \textbf{(111)}$$

that is very similar to the typical values of AU for the fuel cells. This is due in particular to the fact that the cathode channel does not allow an excessive dispersion of the air, that in large part is able to reach the cathode electrode.

It is possible to compare the performances of the fuel cell fed by syngas with the operation of the same cell, fed by an equivalent amount of hydrogen. To compare the two configurations, a molar flux of pure hydrogen able to deliver the same number of electrons delivered by the syngas has been considered. The molar flux at the anode side reduces therefore from the previous $1.12 \cdot 10^{-3}\ mol/s$ of syngas to $4.06 \cdot 10^{-4}\ mol/s$ of hydrogen.

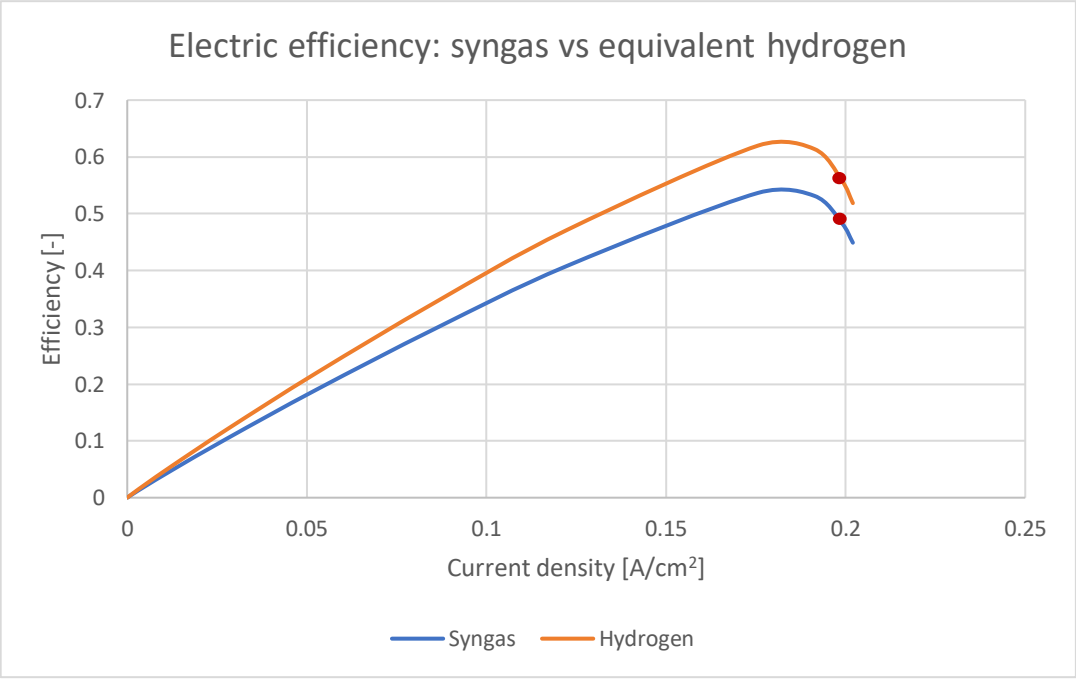

Figure 4.4. Electric efficiencies of fuel cell fed with syngas and equivalent hydrogen

The hydrogen would have a higher efficiency of conversion, even if also the real syngas shows, in general, good performances. However, the working condition at 0.7V imposes to work in the last region of the curve, where the efficiency curve has an abrupt decrease. It is clear therefore that the operation in this point is not a good choice from the point of view of the performances, even if it still remains quite high, as it can be seen in the Table 4.2.

Fuel considered	Efficiency at 0.7V	Maximum efficiency
Syngas	48.4%	53.7%
Equivalent hydrogen	55.9%	62.0%

Table 4.2. Electric efficiencies of SOFC fed with syngas and equivalent hydrogen

To obtain the same efficiency but to avoid the operation in the final region dominated by concentration overvoltages, it could be useful to operate in a different point. The solution could be the increase of the voltage, but a too high value of voltage can lead to operate in a point characterized by low electric efficiency. A trade off must be found in order to find the best operating condition. One possibility is to work at about V=0.95V, that would guarantee the operation in the linear region of the curve (i.e., reduced fuel starvation issues) and an efficiency value still quite high.

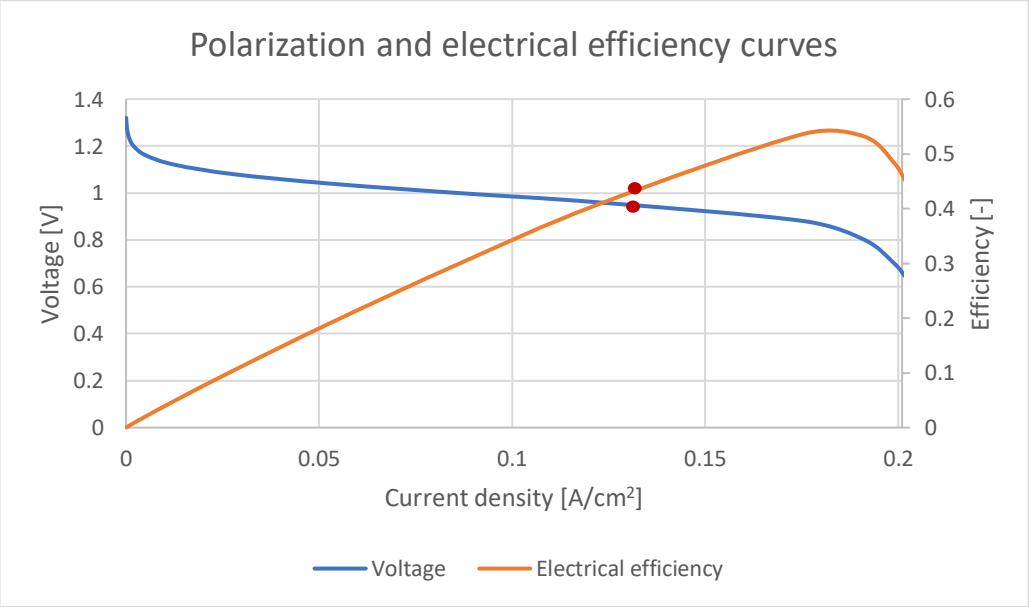

Figure 4.5. Operating conditions at V=0.95V

In this way, the current density will be around 0.13A/cm^2 and the output power will be 8.5W: therefore, even it is lower than before, the required power would still be achieved. On the other hand, the electrical efficiency will decrease, from 48.4% to 42.6%. The comparison between the performances is shown in the table below.

Parameter	Operation at 0.7V	Operation at 0.95V
Current density	$0.20\ A/cm^2$	$0.13\ A/cm^2$
Electrical efficiency	48.4%	42.6%
Output power	$9.59\ W$	$8.44\ W$

Table 4.3. Performances comparison between the two operating points

Even if the electrical efficiency is reduced, this could be a good configuration for the operation of the fuel cell system.

4.1.1. Temperature distribution

The analysis of the operation of the fuel cell must be completed with the evaluation of the temperature distribution inside the system. The map of the temperature inside the cell is represented in Figure 4.6.

The highest temperatures are reached inside the anode channel, where the maximum temperature reached is slightly less than 820°C. In the electrolyte and in the two electrodes the maximum temperature reached is around 817°C. The minimum can be found in the inlet side of both anode and cathode channels. Therefore, the materials of the three main components (electrolyte, anode and cathode electrodes) are subjected to a temperature gradient of about 15°C along the total length of the cell.

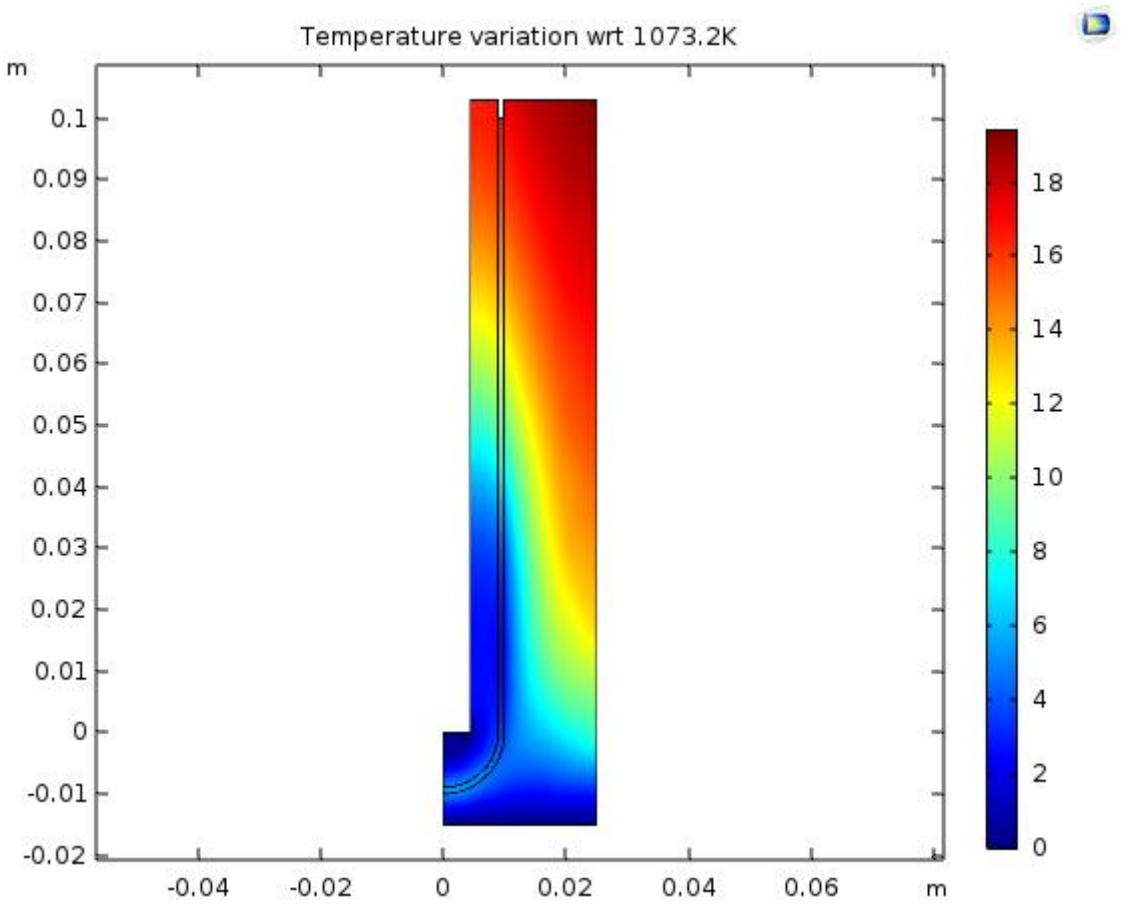

Figure 4.6. Temperature distribution in the fuel cell

4.2. Improved configuration: SOFC operation with syngas

The results obtained in the nominal configuration are poorly satisfactory. In order to improve the configuration maintaining the same design one possibility could be to increase the inlet velocities, and therefore the inlet molar flux, in order to increase consequently the output power. This will represent an improvement from the point of view of the electrical power produced, but not from the point of view of the performances in terms of fuel utilization, since the fuel losses cannot be reduced without a change in the channel structure. However, the impact of fuel losses could be reduced inserting a system of fuel recycling.

Different values of inlet velocities have been applied, in order to find the best configuration leading to a current density of about 0.7 A/cm^2 at a voltage of 0.7 V. The value of voltage of 0.7V is still considered the nominal point of operation, successively the possibility whether to change or not the operating point will be evaluated.

The velocity values are obtained iteratively, and the operating conditions considered are the following:

Configuration	Anode inlet velocity	Cathode inlet velocity
Case 1 (Nominal configuration)	0.05 m/s	0.4 m/s
Case 2	0.4 m/s	1 m/s
Case 3	0.8 m/s	3 m/s
Case 4	1.5 m/s	4 m/s

Table 4.4. Operating conditions for the four configurations

In this way, exploring various values of inlet velocity it is possible to understand how the current density varies according to it. This analysis can be useful in order to assess the best operating condition at which the cell can be made to operate.

The operation of the fuel cell in the different conditions is analysed thanks to the polarization curve.

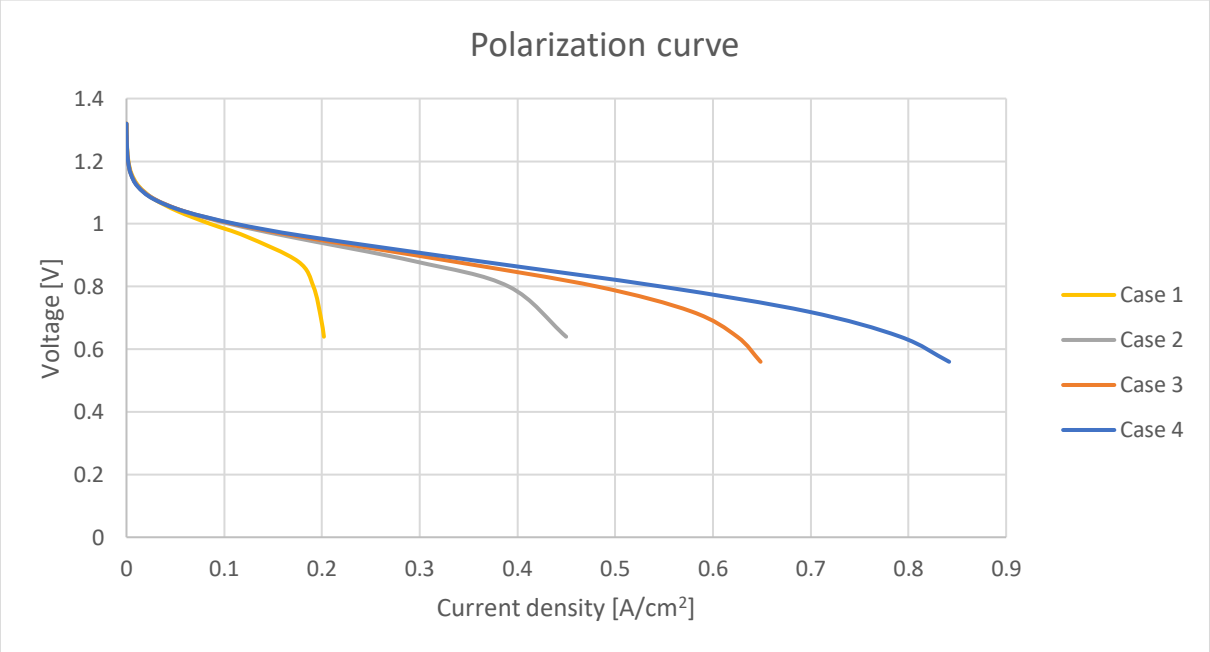

Figure 4.7. Polarization curves in different configurations

Increasing the inlet velocity, the current densities increase as well: in particular the region dominated by the concentration losses is shifted towards higher values of current. If 0.7V is considered as the nominal operating voltage of the fuel cell, from Figure 4.7 it can be observed that the current density values are the following:

Configuration	Current density at 0.7V
Case 1 (Nominal configuration)	0.20 A/cm^2
Case 2	0.43 A/cm^2
Case 3	0.59 A/cm^2
Case 4	0.72 A/cm^2

Table 4.5. Current densities in different operating conditions

The first configuration in which the value of around 0.7 A/cm^2 is reached is the 4th case, while the others show lower values. Also the 3rd configuration leads to a quite high current density value, around 0.6 A/cm^2, but the last configuration is the first one in which the current density value at 0.7V is found in the last part of the ohmic region and not in the concentration one. Since it is better to work in the central zone of the polarization curve to avoid issues linked to fuel starvation the 4th configuration could be considered the best one.

This configuration is now analysed with higher detail.

4.2.1. Case 4: operation and temperature distribution

As it is analysed before, the 4th case is the best one in term of exploitation of the possibilities of the cell. A further increase in the velocity will lead to higher current density values, but too high velocity values could be not suitable for the operation of a SOFC.

Operation

The 4th case study therefore is analysed. The polarization curve and the power curve with respect to the current density are shown below.

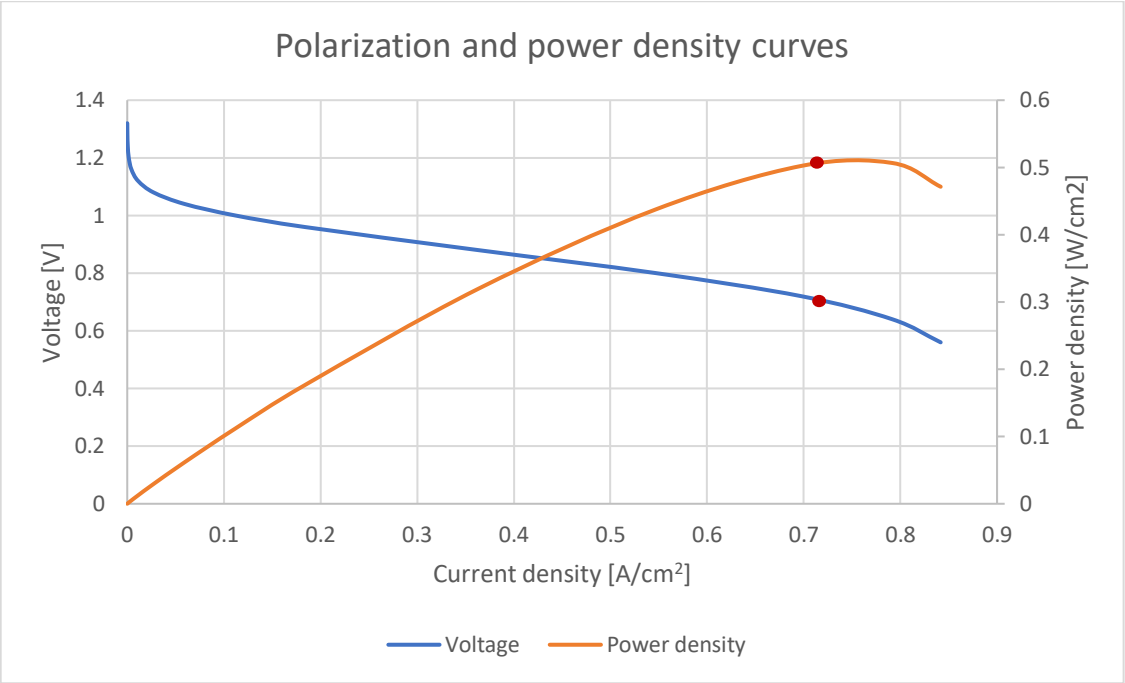

Figure 4.8. Polarization and power density curves

The operation at 0.7V is very close to the maximum value of power reached, that corresponds to the point of the maximum efficiency. Therefore these operating conditions can lead to a good exploitation of the device. This configuration allows to produce an output electric power of about 34.8W, a great increase with respect to the nominal initial configuration.

Also in this case, the efficiency of the SOFC fed by syngas can be compared to the efficiency that would be reached in case of feeding with pure hydrogen.

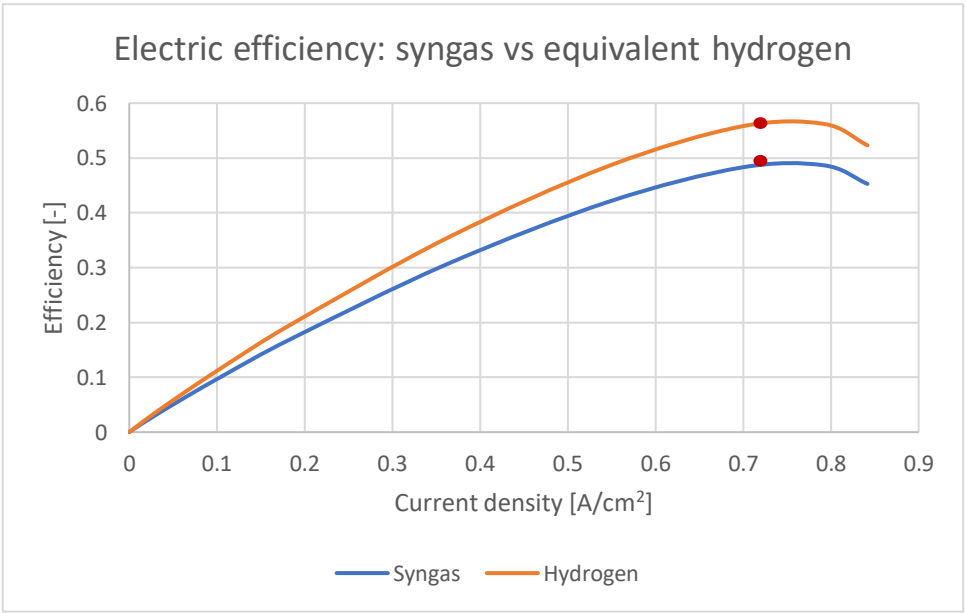

Figure 4.9. Electric efficiencies of syngas and equivalent hydrogen

The feeding with pure hydrogen would lead to higher efficiency, since with a lower amount of fuel the current density obtained would be the same. Anyway the performances of the cell when fed with syngas are in the order of 50%.

Fuel considered	Efficiency at 0.7V	Maximum efficiency
Syngas	48.5%	48.7%
Equivalent hydrogen	56.0%	56.2%

Table 4.6. Efficiencies comparison between syngas and equivalent hydrogen

In this configuration therefore, it would be possible to operate with an efficiency practically equal to the maximum one.

Anyway, in order to move away from the region dominated by concentration losses, again a higher value of voltage can be chosen, like 0,8V, so to avoid an excessive decrease of the electric efficiency. If we decide to choose this value as the new operating point, the power and the efficiency would change, as it is shown in the table

Parameter	Operation at 0.7V	Operation at 0.8V
Current density	0.72 A/cm^2	0.55 A/cm^2
Electrical efficiency	48.5%	42.1%
Output power	34.77 W	30.16 W

Table 4.7. Performances comparison between the two operating conditions

The operation at 0.8V would represent a decrease in terms of efficiency and output power, but could be less subject to fuel starvation phenomena.

Temperature distribution

The temperature distribution (in particular the variation with respect to the operating temperature of 800°C) inside the cell is shown in Figure 4.10.

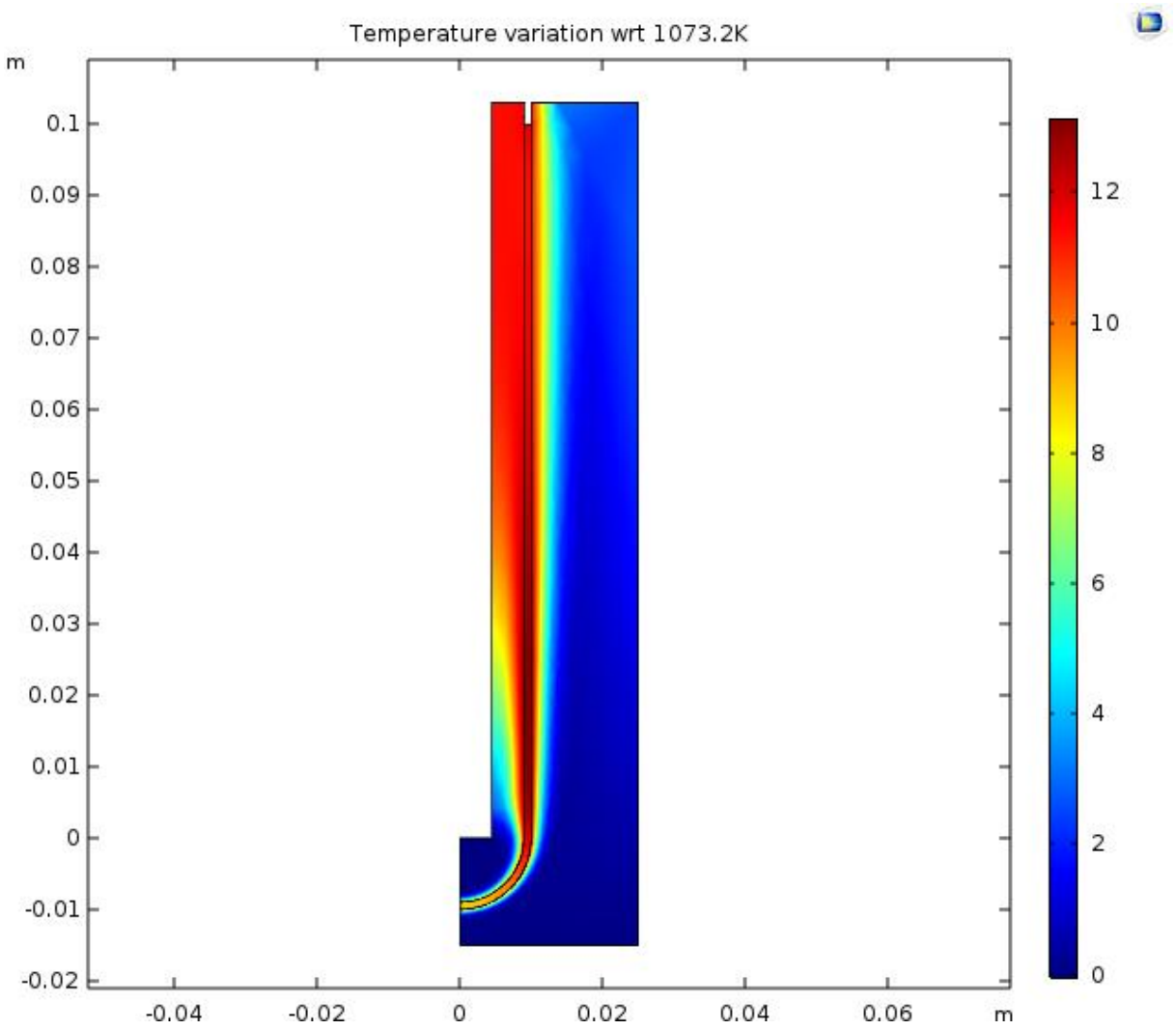

Figure 4.10. Temperature distribution in the fuel cell

The highest values of temperatures are reached inside the cathodic channel, where the flow is more confined. Anyway, the maximum temperature reached in the three components (electrolyte, anode and cathode electrodes) is around 813°C.

4.2.2. Operation with different temperatures

The operation of the fuel cell can be studied in different operating conditions to evaluate how the system is able to respond at temperature and pressure variations. Concerning the first one, an increase of the operating temperature is expected to increase the performances of the cell, while a decrease will cause a reduction of the current density that can be obtained and therefore of the output power. On the other hand, the choice of a higher temperature requires the use of more resistant and therefore more costly materials, increasing thus the total cost of the system.

The operating temperatures considered are four (including the nominal temperature of 800°C): 650°C, 700°C, 750°C and 800°C. Those values of temperature have been chosen since the state of the art of the solid oxide fuel cells nowadays is aiming to reach lower temperatures towards the 600°C degrees, and not to increase further the value towards 900°C. The choice of temperatures lower than 800°C therefore could be coherent with the technological trend.

All the other parameters are maintained constant.

The results are shown below.

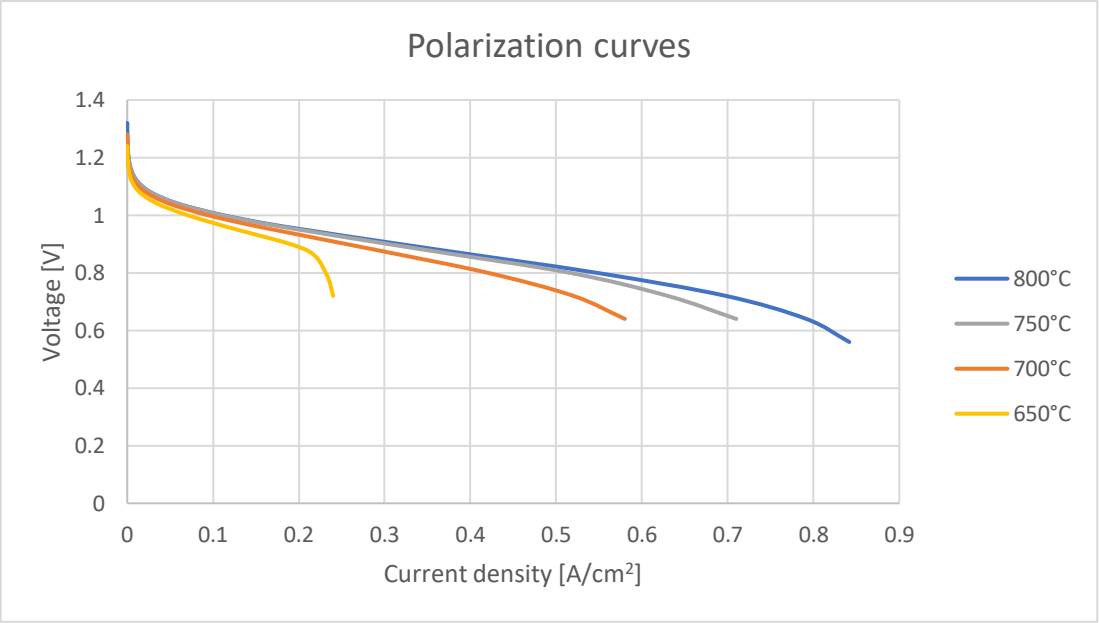

Figure 4.11. Polarization curves at different operating temperatures

The effect of temperature is particularly visible on the curve at 650°C and at high value of current densities. An increase of 50°C only from 650°C to 700°C leads to a dramatic increase in the cell performances and in the current density values that it is able to extract. It is important to notice that the temperature variation affects not only the electrochemical reactions kinetics, but also the kinetics of the SMR and WGS reactions, changing the concentration of syngas components. Actually the SMR is an endothermic reaction, and decreasing the temperature the production of H_2 and CO are less favoured, while the WGS is an exothermic reaction, with an opposite behaviour.

Configuration	Current density at 0.7V
650°C	0.24 A/cm^2
700°C	0.54 A/cm^2
750°C	0.65 A/cm^2
800°C	0.72 A/cm^2

Table 4.8. Current densities at different operating temperatures

According to the results, 650°C seems to be a too low temperature for a good operation of the cell, due to the strong reduction of the current density value. Instead, 700°C and 750°C, even if do not allow to reach the same values obtained at the nominal temperature of 800°C, can be considered as good alternatives.

4.2.3. Operation with different pressures

As the increase of temperature implies an increase in the performances of the cell, so does the pressure, whose increase can lead to an increment in the current densities. In this case, three different values of pressure are studied, including the nominal one: 1atm, 2atm and 5atm.

The results are shown in the Figure 4.12.

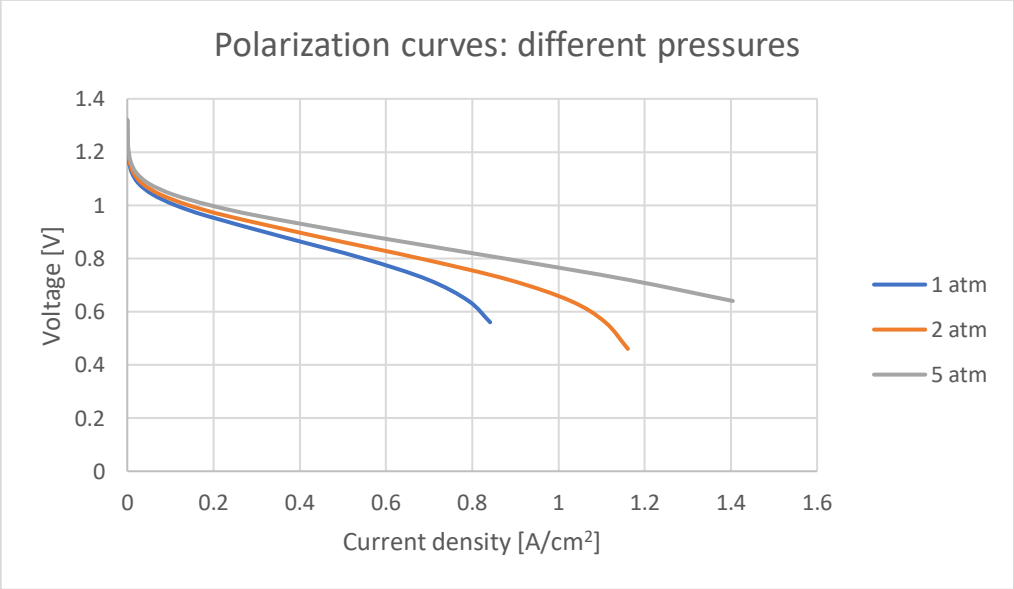

Figure 4.12. Polarization curves at different operating pressures

Configuration	Current density at 0.7V
1atm	0.72 A/cm^2
2atm	0.92 A/cm^2
5atm	1.22 A/cm^2

Table 4.9. Current densities at different operating pressures

As expected, the increase of pressure increases the current density values. In particular, a pressure equal to 2atm already allows to reach current densities higher than 1 A/cm^2 in the last region of the curve. Additionally, it permits to move away the operating point at 0.7V from the region characterized by the concentration overvoltages, therefore it could be a good compromise between the operation at 1atm and 5atm.

Also in this case it must be underlined that the increase of pressure affects the equilibrium of the heterogeneous reactions. In particular, for the SMR, since the products present a higher number of moles, the increase of pressure does not favour the production of H_2 and CO.

4.2.4. Operation with different conditions: comparison

The operation under different temperature and pressure conditions leads to very different results. In general, the decrease of temperature decreases as well the current density values that can be reached, and an increase of pressure allows to reach higher current density values. The main results obtained are summed in the following tables.

Temperature (p=1atm)	Current density
650°C	0.24 A/cm^2
700°C	0.54 A/cm^2
750°C	0.65 A/cm^2
800°C	0.72 A/cm^2

Table 4.10. Current densities with varying temperature

Pressure (T=800°C)	Current density
1 atm	0.72 A/cm^2
2 atm	0.92 A/cm^2
5 atm	1.22 A/cm^2

Table 4.11. Current density with varying pressure

An excessive decrease in the working temperature can affect too much the performances of the cell, while a too high pressure value could introduce important complexities in the coupling between the gasification process and the SOFC operation. Therefore, the configurations that could be taken into account as possible alternatives for a change in the operating conditions could be the following:

- Operation at 750°C, 1atm;
- Operation at 800°C, 2atm.

4.3. Possible design improvement

As seen in the previous sections, the main issue affecting the performances of the cell is the design and the geometry. The relatively great dimensions of the anode channel and of the fuel cell in general have a negative impact on the dispersion of both air and fuel flows. Therefore, a possible improvement can be represented by the choice of a different geometry: in particular, the choice of a narrower anode flow channel, which could better funnel the fuel inside the porous structure of the electrode. In this way, the exploitation of the fuel flow would be more efficient, leading to higher performances, both regarding the fuel utilization and the electrical efficiency.

The operation of the fuel cell with a channel flow inlet section of 1.5cm of radius is analysed: in this way, the thickness of the channel will be smaller, reducing the fuel dispersion.

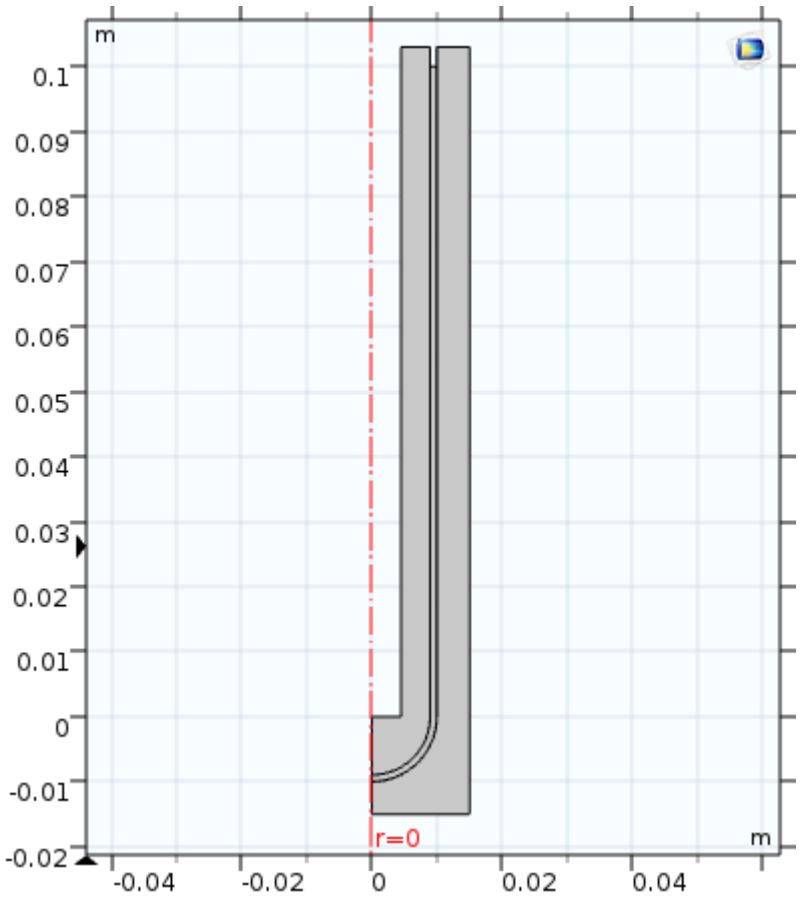

Figure 4.13. New possible geometry

In this analysis, the same inlet velocities as the nominal configuration has been applied: having a smaller anode inlet section, the molar flux of anode fuel will be reduced. The molar flux passes from $1.12 \cdot 10^{-3}\ mol/s$ of the nominal case to $4.02 \cdot 10^{-4}\ mol/s$.

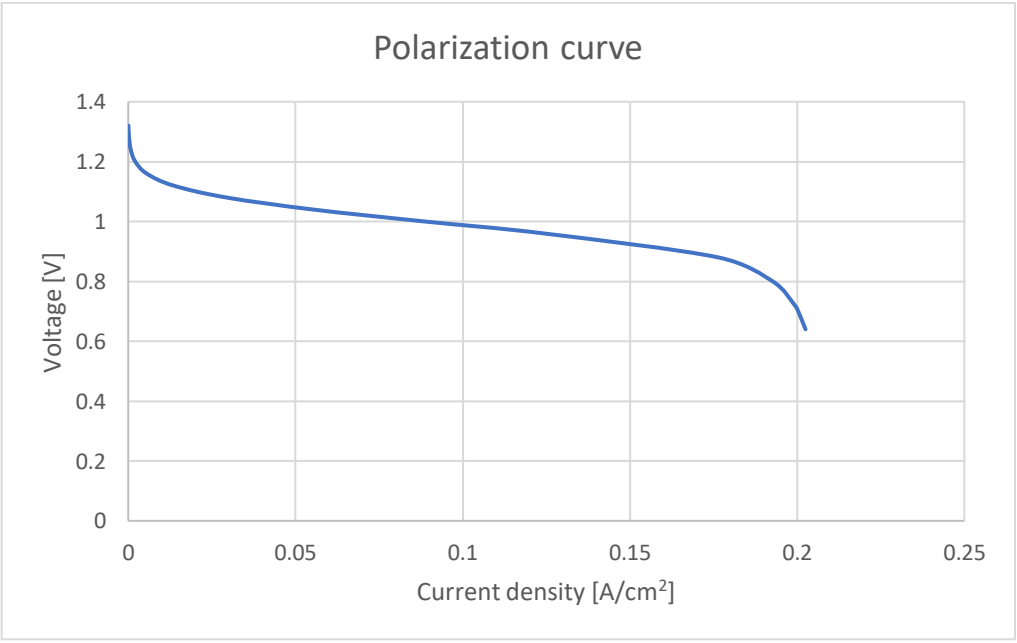

Figure 4.14. Polarization curve of the cell, considering a different geometry

In this case, the output power obtained at 0.7V (operating point that can be shifted towards higher values of voltage, in order to work in the linear region of the curve) is slightly higher than the original configuration (9.66W), but now this power has been obtained using a molar flux of fuel that is about one third of the initial flux. This represents an important improvement from the point of view of the exploitation of the total fuel. The fuel utilization, that initially was equal to 17.5%, now is:

$$FU = 48.9\% \tag{112}$$

The reduction of the anode channel represents therefore a great improvement from the point of view of the utilization of the fuel. Also the electric efficiency referred to the total inlet fuel increases, from 8.5% to 23.7%.

A change in the geometry of the system itself therefore could constitute an important step in order to increase the performances of the cell, that could become even higher if a fuel recycle were introduced.

4.4. Gasification

For the gasification model, a further variation on the domain has been made, as it can be seen in Figure 4.15.

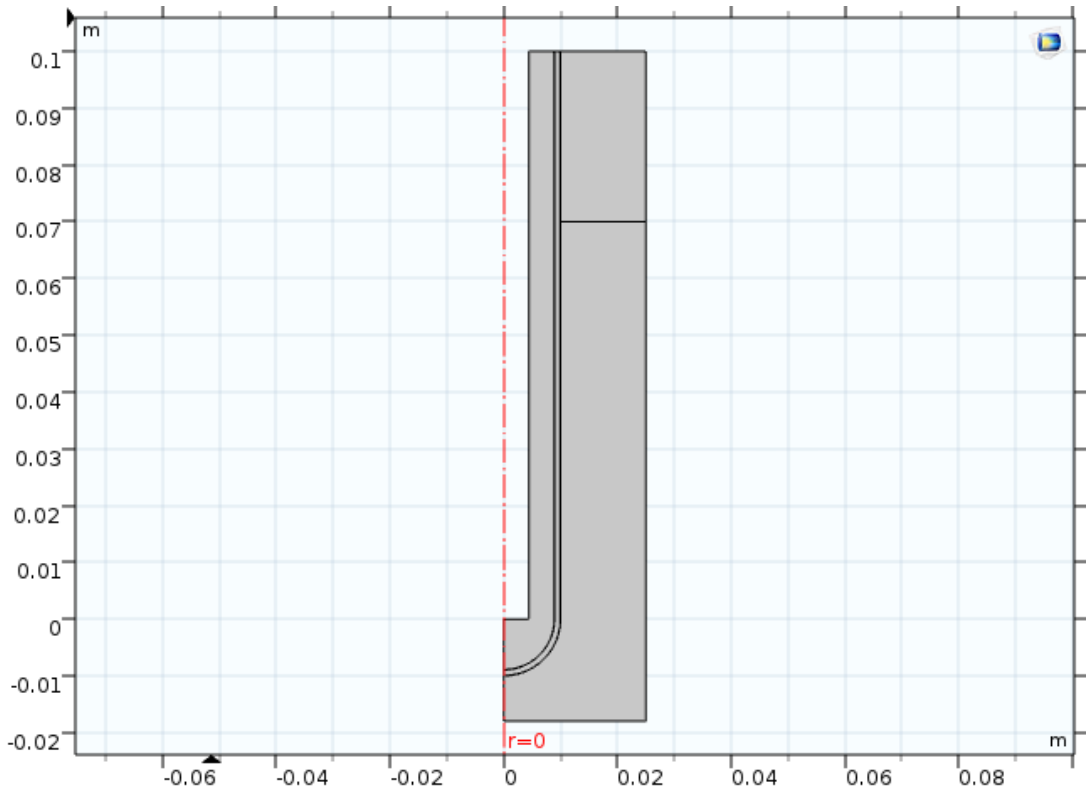

Figure 4.15. Geometry used in the gasification model

As it can be observed, the anode channel has been divided into two different regions. In the region below, it is assumed that the biomass is present, in accordance with the project design; above this zone, only the gaseous species produced are present. Therefore, the mass conservation of solid species (modelled with the Ordinary Differential Equations on the software) is applied exclusively in the below region.

The gasifying agent (the CO_2) is injected through the lower side, as in the previous case for the anodic flow inlet.

For the initial conditions it was assumed the presence of the CO_2 and, in the region occupied by the biomass, the moisture contained in the solid matter. Also the moisture is assumed to enter continuously, carried inside the reactor by the biomass.

For the gasification, a biomass feeding rate of 15kg/h for the total reactor has been considered, that corresponds roughly 0.6kg/h for each fuel cell control volume. The gasifying agent (the CO_2) enters with a velocity of around 0.9m/s. Some of the main parameters used are listed in Table 4.12.

Biomass feeding rate (total reactor)	15 kg/h
Gasifying agent velocity	0.9 m/s
Biomass density	573 kg/m^3
Biomass moisture content	ca. 10% wt.

Table 4.12. Main parameters used for gasification model

The results of the gasification process are the following:

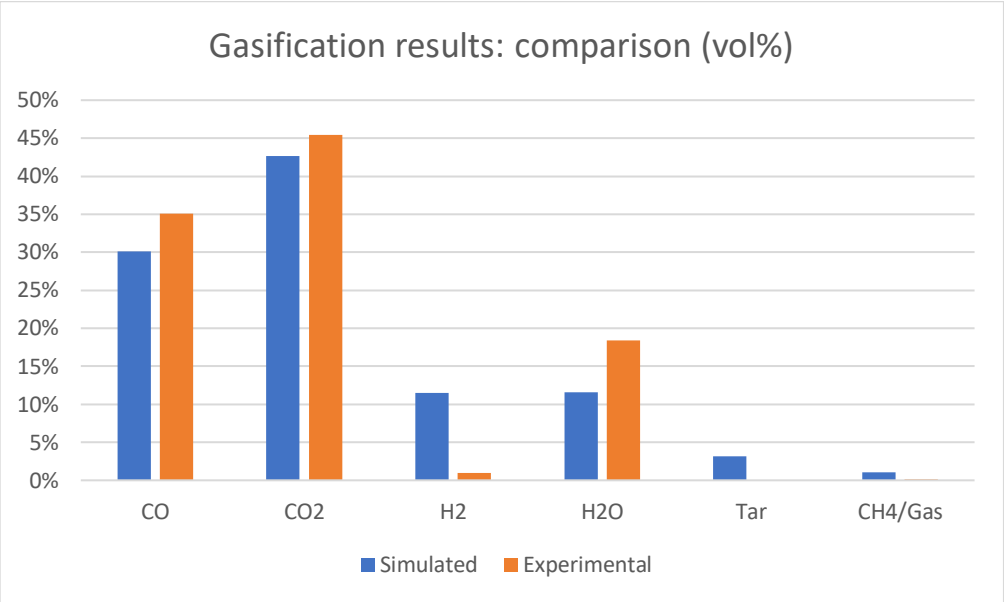

Figure 4.16. Gasification results: molar composition of the producer gas

Although the most present compounds are respected (CO and CO_2 account for around 75% of the total producer gas in both cases), the results are not completely in accordance with the experimental values, in particular for which concerns hydrogen and water content. This could be mainly due to the not precise data related to the biomass chosen for the simulation: actually, those values have been found from literature and can be different from the real characteristics of biomass used in the experimental part. Moreover, as it was stated in the model section, the relations proposed by Guizani to simulate the gasification started from the assumption that the char was composed by carbon solely. This could lead to the discrepancies shown in the graph above.

Concerning the high heating value, in literature values of HHV for the olive kernel are available. Anyway, those values are referred to the particular composition of the biomass itself, in which carbon constitutes a fraction. In this work, in order to remain coherent with the previous hypothesis, the value of HHV for the biomass has been evaluated considering the formula below:

$$HHV\left[\frac{MJ}{kg}\right] = 0.341 \cdot C + 1.322 \cdot H - 0.12 \cdot O - 0.12 \cdot N + 0.0686 \cdot S - 0.0153 \cdot ash \quad (113)$$

in which C, H, etc., are the mass fraction in wt% on dry basis. Since the biomass for simplicity has been assumed to be composed by carbon only, the only term left is C=100. Therefore, the HHV becomes:

$$HHV\left[\frac{MJ}{kg}\right] = 0.341 \cdot C = 34.10\frac{MJ}{kg} \quad (114)$$

With this value, it is possible to estimate the efficiency of the gasifier (in terms of cold gas efficiency, CGE) as:

$$CGE = \frac{G_{syngas} \cdot HHV_{syngas}}{G_{biomass} \cdot HHV_{biomass}} \quad (115)$$

As said, the biomass feeding rate is 0.6kg/h; considering the inlet flow rate of CO_2 and the moisture content that the biomass transport inside the reactor, the mass flow rate of syngas can be obtained. Then the HHV of syngas is obtained considering the molar fraction of each fuel present in the producer gas, and the value obtained is:

$$\overline{HHV}_{syngas} = \sum_i y_i \cdot \overline{HHV_i} \cong 113050\frac{J}{mol} \quad (116)$$

$$CGE = \frac{G_{syngas} \cdot M_{syngas} \cdot \overline{HHV}_{syngas}}{G_{biomass} \cdot HHV_{biomass}} = 66.0\% \quad (117)$$

The simulated gasification process therefore is quite efficient and can be a good starting point for the operation of the fuel cell.

It is important to notice that changing the operating conditions and the biomass parameters, the gasification result in terms of producer gas composition will change as well. The biomass feeding rate, the inlet velocity of the gasifying agent, the moisture content and the operating temperature and pressure are the main parameters affecting the resulting composition. Since in previous sections an evaluation of the fuel cell performances in different operating conditions has been made, it could be useful to analyse how the producer gas composition varies with different operating conditions, to understand if a change in the operating temperature and pressure could represent an improvement. As previously stated, two different operating conditions have been analysed: the operation at 750°C and 1atm, and the operation at 800°C and 2atm. The results are shown in Figure 4.17.

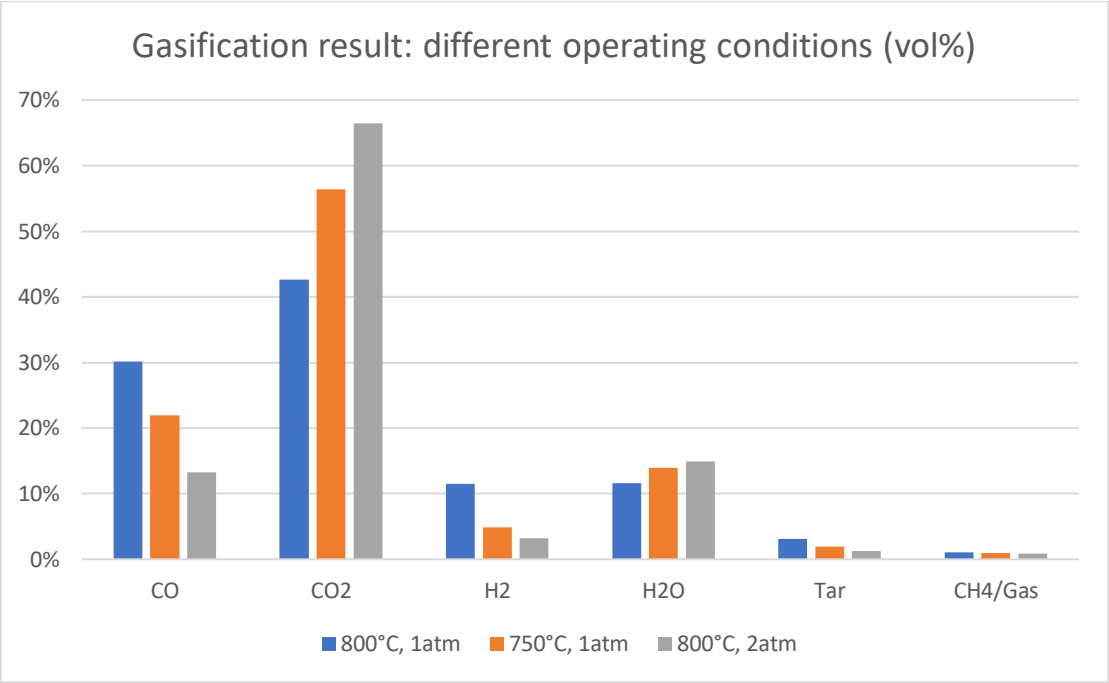

Figure 4.17. Producer gas composition under different operating conditions

The results show an important variation in the syngas composition: the molar fraction of carbon monoxide drops with the decrease of temperature and the increase of pressure, with a great increase in the carbon dioxide presence. Also the hydrogen content is strongly reduced. The syngas produced would be less rich in fuel like CO and H_2, with higher amount of compounds already oxidized, like CO_2 and H_2O, with a consequent reduction of the chemical energy that could be exploited.

Therefore, the best operating condition is represented by the nominal one, at 800°C and 1atm.

4.5. Integration of gasification and SOFC

After having set the gasification parameters for the description of the gasification model, now the integration between the gasification process and the SOFC operation must be performed. The producer gas, whose composition has been obtained before, reaches now the anode electrode up to the catalyst layer, and undergoes the electrochemical oxidation.

The differences between this configuration and the nominal one presented before, in which the SOFC was fed by syngas, are not only the different gas composition (that here is richer in hydrogen content) but also the different structure of the external fluid channel, that now is assumed to be filled with biomass with a certain porosity.

The polarization curve is shown in Figure 4.18, while in Figure 4.19 a comparison between the polarization curve obtained with the previous analysis on the fuel cell fed with syngas and the one referred to the coupling with the gasification process can be observed.

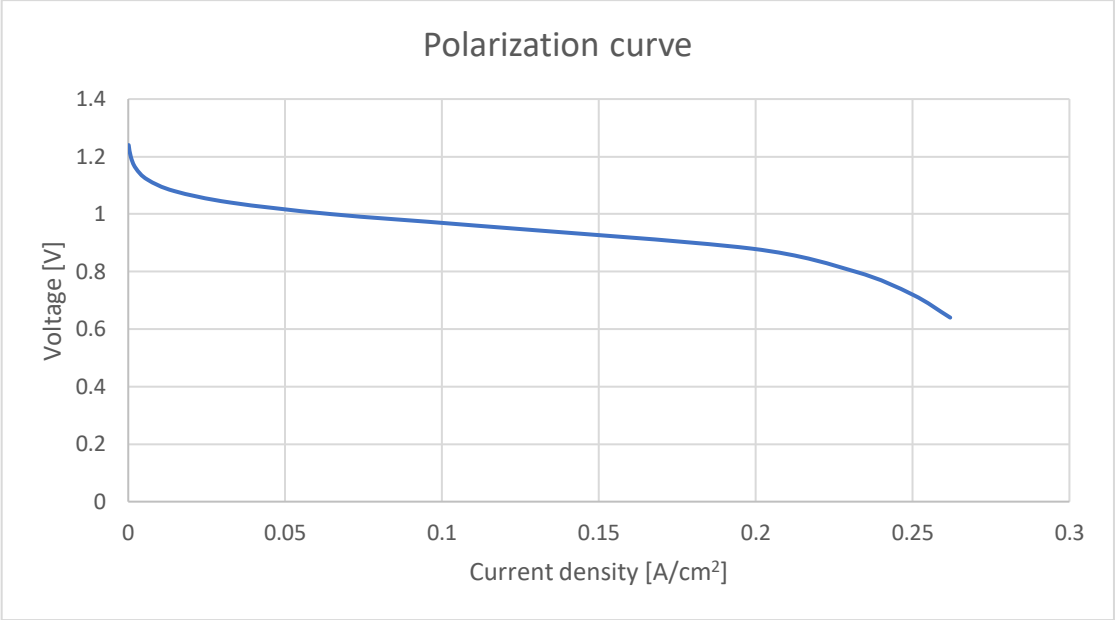

Figure 4.18. Polarization curve of the SOFC coupled with gasification process

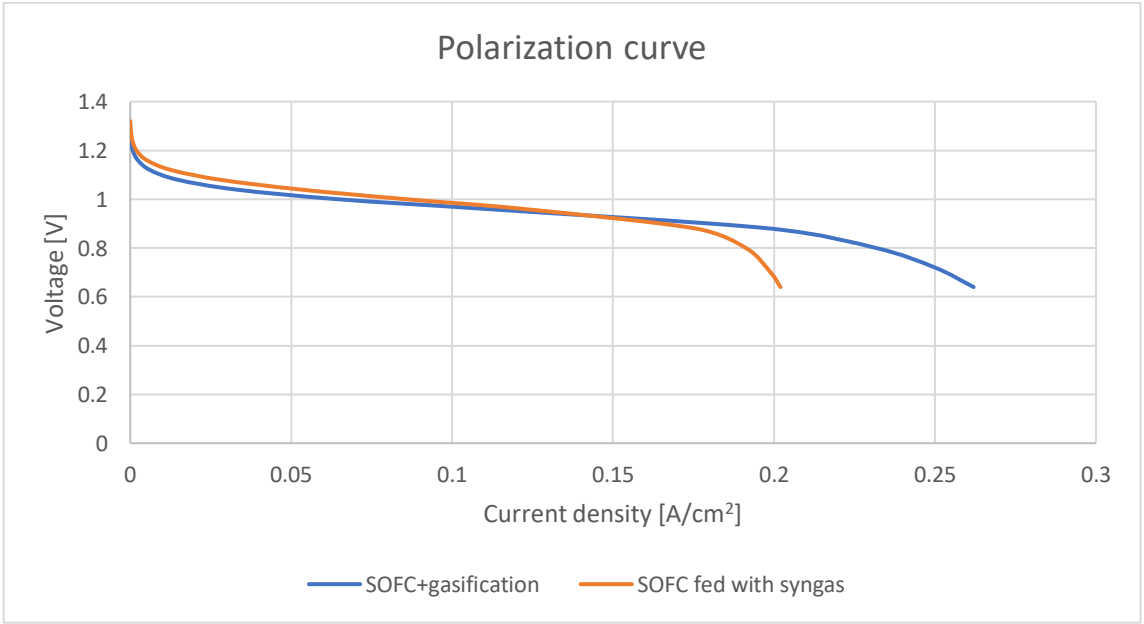

Figure 4.19. Comparison between the polarization curve of the cell fed by already produced syngas and the one of the cell coupled with the gasification process

How can be seen from the figure, the two curves are very similar in the first part, but reaching lower values of voltages they differ consistently. The coupled system allows to obtain a production higher than 8W: actually, reaching a current density of around 0.25A/cm^2, the power produced is around 12.3W. This can be due to a different molar flux able to reach the anode electrode, but also to the different fuel composition, that in the COMSOL simulation appears to be much richer in hydrogen.

This result anyway can be optimistic: the model does not take into account some criticalities that can occur during the real operation of the system. Carbon deposition, tar and ash formation and, in general, the presence of impurities inside the producer gas can affect negatively the performances of the cell.

Concerning the efficiency of the SOFC, in this case the fuel utilization and the efficiency considering the total syngas produced is even lower than before (FU=0.6%, η_{el}=0.3%), and therefore the efficiency of the total system (gasification process + SOFC) would become around η=0.2%. The same consideration made for the operation of SOFC fed with syngas can be made, therefore considering only the amount of syngas that effectively manages to reach the anode electrode of the fuel cell. Also in this case the electric efficiency increases:

$$\eta_{el,SOFC} = 50.1\% \quad \textbf{(118)}$$

Considering the complete system, the overall efficiency can be evaluated as:

$$\eta_{Biomass \rightarrow electricity} = \eta_{el,SOFC} \cdot CGE = 0.501 \cdot 0.660 = 0.330 = 33.0\% \quad \textbf{(119)}$$

This number therefore shows that the overall system has a quite good efficiency from the point of view of the technologies exploited. Nevertheless, the dramatically low efficiency of the complete system cannot be forgotten: actually, even the technologies show good performances, the losses in terms of fuel dispersion are high. This issue could be solved introducing a fuel recycle, or in alternative gasifying the biomass in a different reactor and introducing the producer gas in the fuel cell.

4.5.1. Temperature distribution

The last aspect to analyse is the temperature distribution inside the fuel cell, that will combine the heat generated by the fuel cell operation and by the reactions occurring between the gaseous species produced.

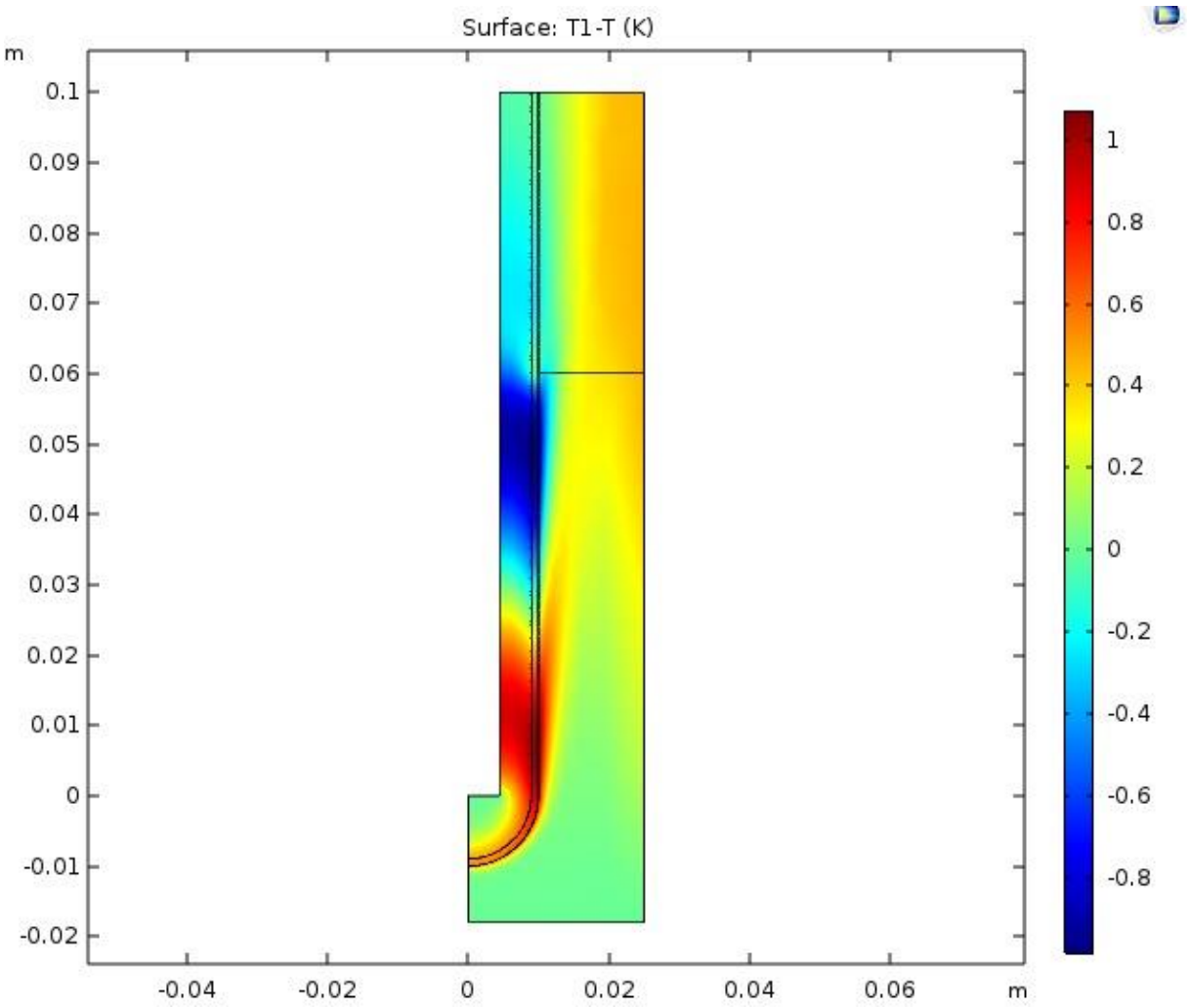

Figure 4.20. Temperature variation with respect to 800°C

In this case, very small variations of temperature with respect to the operating temperature of 800°C can be observed. This could be due to the endothermic reactions occurring between the gaseous species, that behave as thermal sinks. Actually the steam methane reforming is endothermic, and since in this configuration the amount of methane is higher than in the case of the already produced syngas, this could have a higher impact on the temperature of the system. Additionally, gasifying directly at the anode side, the syngas composition can be not uniform, and also the electricity production at the anode side can be not uniform and lead to such distribution.

Anyway, this evaluation is highly approximated, since only the WGS and SMR have been considered, and since it was assumed that the gasification process was completely sustained from the external with a proper heat source.

5. CONCLUSIONS

The aim of this thesis was the development of a model to describe the integration between biomass gasification and solid oxide fuel cell operation. This has been achieved realizing a 2D axisymmetric model on COMSOL Multiphysics®, 5.3 using various physics to describe the phenomenon.

The model has been used to analyse firstly the operation of the fuel cell when fed with syngas composed by CO, CO_2, H_2, H_2O and CH_4, to understand the operating conditions at which the system was able to produce a power equal to 8W, evaluating also the electric efficiency of the system. A configuration able to produce around 9.5W per cell has been found. Then, a possible change in the geometry has been proposed, in order to improve the exploitation of the fuel. After the reduction of the anodic flow channel radius from 2.5cm to 1.5cm, the results showed an increase in the fuel utilization from 17.8% to 48.9%. This means higher performances of the cell and a better exploitation of the fuel.

After that, the gasification simulation has been performed. Also in this case, in absence of experimental data regarding the biomass, some assumption have been made in order to obtain a resulting syngas composition as close as possible to the initial data available. The final composition achieved still presented differences if compared to the original data, but this could be due to the absence of more precise data about the biomass and the gasification operating conditions.

Finally, the complete integrated system has been realized, obtaining the polarization curve of the fuel cell fed with the syngas produced in the modelled gasification. The current density obtained at 0.7V was found to be higher than the one obtained in the nominal configuration, therefore the 8W of power production should be granted. Anyway, some criticalities linked to the integration of the biomass gasification with the SOFC operation has been neglected. The real operation will be affected by phenomena of carbon deposition, production of ashes and tars that could affect the operation of the fuel cell. For this reason, an accurate analysis about the impact of these issue on the fuel cell operation should be developed in future.

5.1. Future work

There are many aspects that should be further analysed, in order to obtain a reliable model that could fully describe the process.

First of all, the carbon deposition problem is an important aspect that is worth analyzing. The deactivation of the catalyst is an issue that must be analysed both in the configuration with syngas but also in the integration with the gasification process. Additionally, not only the carbon deposition issue, but also the tar impact and the ash generation and deposition are criticalities that must be deeply studied, to avoid operation problem.

Also concerning the gasification process, some improvement has to be done. In particular, an analysis on the biomass matter would allow to use more correct parameters, in order to obtain a more descriptive model.

Eventually, a design variation can be useful in order to improve the efficiency of the system and also to avoid the criticalities related to the biomass presence all around the fuel cell.

BIBLIOGRAPHY

[1] Z. Ud Din and Z. A. Zainal, "Biomass integrated gasification-SOFC systems: Technology overview," *Renew. Sustain. Energy Rev.*, vol. 53, pp. 1356–1376, 2016.

[2] "https://ec.europa.eu/eurostat/web/main/home." [Online]. Available: https://ec.europa.eu/eurostat/web/main/home.

[3] C. Parisius, "DB-SOFC DB-SOFC ERANETMED2-72-246," pp. 1–45, 2020.

[4] S. Kakaç, A. Pramuanjaroenkij, and X. Yang, "A review of numerical modeling of solid oxide fuel cells," vol. 32, pp. 761–786, 2007.

[5] N. Steiner, D. Marra, M. Sorrentino, C. Pianese, K. Wang, D. Hissel, M. C. Pe, M. Monteverde, P. Cardone, and J. Saarinen, "A Review on solid oxide fuel cell models," vol. 6, 2011.

[6] R. Bove, P. Lunghi, and N. M. Sammes, "SOFC mathematic model for systems simulations . Part one : from a micro-detailed to macro-black-box model," vol. 30, pp. 181–187, 2005.

[7] P. Aguiar, C. S. Adjiman, and N. P. Brandon, "Anode-supported intermediate temperature direct internal reforming solid oxide fuel cell . I : model-based steady-state performance," vol. 138, pp. 120–136, 2004.

[8] F. Calise, M. Dentice, and G. Restuccia, "Simulation of a tubular solid oxide fuel cell through finite volume analysis : Effects of the radiative heat transfer and exergy analysis," vol. 32, pp. 4575–4590, 2007.

[9] X. Xue, J. Tang, N. Sammes, and Y. Du, "Dynamic modeling of single tubular SOFC combining heat / mass transfer and electrochemical reaction effects," vol. 142, pp. 211–222, 2005.

[10] J. R. Ferguson, J. M. Fiard, and R. Herbin, "Three-dimensional numerical simulation for various geometries of solid oxide fuel cells," pp. 1–27.

[11] K. Nikooyeh, A. A. Jeje, and J. M. Hill, "3D modeling of anode-supported planar SOFC with internal reforming of methane," vol. 171, pp. 601–609, 2007.

[12] M. Puig-arnavat, J. C. Bruno, and A. Coronas, "Review and analysis of biomass gasification models," *Renew. Sustain. Energy Rev.*, vol. 14, no. 9, pp. 2841–2851, 2010.

[13] A. Gómez-Barea and P. Ollero, "An approximate method for solving gas – solid non-

catalytic reactions," vol. 61, pp. 3725–3735, 2006.

[14] Z. A. Zainal, R. Ali, C. H. Lean, and K. N. Seetharamu, "Prediction of performance of a downdraft gasifier using equilibrium modeling for different biomass materials," vol. 42, 2001.

[15] K. D. Panopoulos, L. E. Fryda, J. Karl, S. Poulou, and E. Kakaras, "High temperature solid oxide fuel cell integrated with novel allothermal biomass gasification Part I : Modelling and feasibility study," vol. 159, pp. 570–585, 2006.

[16] E. Shayan, V. Zare, and I. Mirzaee, "On the use of different gasification agents in a biomass fueled SOFC by integrated gasifier : A comparative exergo-economic evaluation and optimization," *Energy*, vol. 171, pp. 1126–1138, 2019.

[17] S. McIntosh and R. J. Gorte, "Direct Hydrocarbon Solid Oxide Fuel Cells," *Chem. Rev.*, vol. 104, no. 10, pp. 4845–4866, Oct. 2004.

[18] A. Dicks, *Fuel Cell Systems Explained*. .

[19] "https://www.ceramicindustry.com/articles/86115-ceramic-energy-advances-in-sofc-materials-and-manufacturing." [Online]. Available: https://www.ceramicindustry.com/articles/86115-ceramic-energy-advances-in-sofc-materials-and-manufacturing.

[20] BP p.l.c., "BP Statistical Review of World Energy," London, UK, 2018.

[21] H. Zhu, R. J. Kee, V. M. Janardhanan, O. Deutschmann, and D. G. Goodwin, "Modeling Elementary Heterogeneous Chemistry and Electrochemistry in Solid-Oxide Fuel Cells," *J. Electrochem. Soc.*, vol. 152, no. 12, p. A2427, 2005.

[22] M. Ni, "Modeling of SOFC running on partially pre-reformed gas mixture," *Int. J. Hydrogen Energy*, vol. 37, no. 2, pp. 1731–1745, 2011.

[23] A. Leonide, S. Hansmann, and E. Ivers-Tiffée, "A 0-Dimensional Stationary Model for Anode-Supported Solid Oxide Fuel Cells," *ECS Trans.*, vol. 28, pp. 341–346, Jan. 2010.

[24] H. A. Jakobsen, *Chemical Reactor Modeling: Multiphase Reactive Flows*, Second Edi. 2014.

[25] M. Ni, "2D Heat and Mass Transfer Modeling of Methane Steam Reforming for Hydrogen Production in a Compact Reformer," no. 852, pp. 1–22.

[26] C. Guizani, "Effects of CO2 on the biomass pyro-gasification in High Heating Rate and Low Heating Rate Conditions," Université de Toulouse, 2014.

[27] A. Chaurasia, "Modeling, simulation and optimization of downdraft gasifier: Studies

on chemical kinetics and operating conditions on the performance of the biomass gasi fi cation process," *Energy*, vol. 116, pp. 1065–1076, 2016.

[28] B. Lee, S. Lee, and H. Lim, "Numerical modeling studies for a methane dry reforming in a membrane reactor," *J. Nat. Gas Sci. Eng.*, vol. 34, pp. 1251–1261, 2016.

[29] B. K. Abdalla, S. S. E. H. Elnashaie, S. Alkhowaite, and S. S. Elshishinib, "Intrinsic kinetics and industrial reactors modelling for the dehydrogenation of ethylbenzene to styrene on promoted iron oxide catalysts," vol. 113, pp. 89–102, 1994.

[30] M. Ammar, M. I. A. Mutalib, Y. Suzana, and I. Abrar, "Kinetic model for tar cracking in biomass steam gasification for hydrogen production," no. February 2017, 2016.

[31] C. Sun and U. Stimming, "Recent Anode Advances in Solid Oxide Fuel Cells," *J. Power Sources*, vol. 171, pp. 247–260, Sep. 2007.